Joint Design of Communication, Wireless Energy Transfer, and Control for Swarm Autonomous Underwater Vehicles

Hongzhi Guo, *Member, IEEE,* Zhi Sun, *Senior Member, IEEE,* and Pu Wang

***Abstract*—A swarm of Autonomous Underwater Vehicles (AUVs) can provide richer spatial-temporal information than the traditional single-robot system, which can be used for underwater mapping, exploration, target tracking, among others. However, the limitation of AUVs' battery cannot support persistent services, which restricts AUVs' operating range and mission duration. In this paper, a mobile underwater charging solution is developed that can continuously recharge a swarm of AUVs by using a wireless mobile charger. Magnetic induction-based communication and wireless energy transfer are employed. This paper first shows that by using tri-axis coils, reliable wireless communication and wireless energy transfer without coil orientation losses can be obtained. After that, wireless communication, motion control, and wireless energy transfer are jointly designed for a swarm of mission-driven AUVs. In particular, optimal continuous motion controllers are developed for AUVs to avoid intra-swarm collisions and networking protocols are designed to optimally allocate resources for wireless communication and wireless energy transfer. The proposed approach can guide AUVs to their destinations, while maintaining wireless network integrity and maximizing wireless energy transfer efficiency, upon which the constraints on AUVs' batteries can be eliminated and cheaper and smaller AUVs can be employed for various underwater applications.**

***Index Terms*—Magnetic induction, motion control, swarm AUVs, tri-axis coil, underwater, wireless communications, wireless energy transfer.**

I. Introduction

Although the wireless underwater sensor plays an important role in exploring and monitoring underwater environments, it can only passively sense information at specific locations [2], [3]. It is challenging to model and analyze underwater dynamics based on the limited information provided by static wireless underwater sensors. Mobile Autonomous Underwater Vehicles (AUVs), as an alternative solution, can actively track targets, map underwater pollution, and survey harsh environments. They can adapt to underwater dynamics and provide accurate rich information. In addition, AUVs can accomplish assigned tasks without being remotely controlled by human beings, by which a large number of dull and dangerous tasks can be accomplished autonomously in underwater environments. However, a single AUV has limited energy, communication capability, and computation resources, which significantly limits its operating range. Recently, the cost of AUVs has dramatically reduced due to the development of manufacturing technologies [4], which motivates the employment of swarm AUVs to provide rich spatio-temporal information. As an emerging technology, the swarm AUVs is facing challenges from wireless communication, networking, energy, control, among others.

Swarm AUVs relies on high-speed and low-latency Wireless Communication (WC) to coordinate motion and transmit data. Existing acoustic underwater communications [5] cannot support swarm AUVs since they demonstrate narrow bandwidth and long latency due to the low carrier frequency and the low propagation velocity. Even worse, acoustic signals experience significant multipath fading, which results in noticeable communication errors. The Remotely Operated Underwater Vehicles (ROUV) use cables to tether vehicles for communication and power supply [6]. Although this solution is reliable, the ROUV has a limited operating range and requires human intervention, which is not fully autonomous. As a result, we cannot deploy large-scale ROUV networks to automate dangerous underwater applications. Wireless underwater optical communication can provide high communication speed thanks to its broad bandwidth [7]. However, the requirement of precise alignment of transceivers is hard to achieve in dynamic underwater environments, which results in inferior and unreliable performance. Also, the optical communication link between AUVs can be easily blocked by other AUVs in the same swarm or by underwater objects. Due to above challenges, employing wireless underwater optical communication for swarm AUVs requires complicated coordination, which is not practical yet. Magnetic Induction (MI) communication is an effective solution in low-conductive underwater environments such as lakes and rivers [5], [8]–[11]. It uses long-wavelength electromagnetic signals to reduce attenuation losses and reflections. MI communication can provide low-latency high-speed data transmission and, thus, it can meet the communication requirements of swarm AUVs.

Besides wireless communication, the limited available energy also restricts AUVs' operating range and mission duration. This is a critical problem for target tracking and many other crucial applications. If AUVs return to their abovewater dispatch station for recharging, they may fail in tracking their targets. In [12], underwater docking stations are used to charge

Part of the results has been presented in [1]. This work was supported in part by The Thomas F. and Kate Miller Jeffress Memorial Trust, Bank of America, Trustee, and the National Science Foundation under Grant No. 1652502, 1936599, and 1953460. Hongzhi Guo is with the Engineering Department, Norfolk State University, Norfolk, VA, 23504, Email: hguo@nsu.edu. Zhi Sun is with the Electrical Engineering Department, University at Buffalo, State University of New York, Buffalo, NY, 14260, Email: zhisun@buffalo.edu. Pu Wang is with the Department of Computer Science, University of North Carolina at Charlotte, Charlotte, NC, 28223, Email: pu.wang@uncc.edu.

mobile AUVs. The mobile charger provides a platform to dock and recharge an AUV. Although it can achieve high energy transfer efficiency and does not require the return of AUVs, this approach demands high accuracy of alignment and cannot charge multiple AUVs simultaneously. As mentioned in [12], the underwater mobile docking station is under development and it is not available yet.

Wireless Energy Transfer (WET) has been extensively used to recharge electronic devices and electric vehicles [13], [14]. It does not require direct contact with the charger and can charge multiple devices simultaneously [15]. Hence, WET is a promising solution to charge a swarm of AUVs. A mobile charger with sufficient energy can be dispatched from a surface station to recharge AUVs wirelessly. As shown in Fig. 1, there are two WET strategies in underwater. The static surface station is used to recharge AUVs and mobile chargers who have accomplished their missions and returned to the station, while the mobile charger is used to recharge mobile AUVs who are serving on their missions and cannot stop to be recharged. In this paper, we focus on the *mobile* case and develop a simple but reliable transmission policies for WET using tri-axis coils.

WC and WET for mobile AUVs are challenging since AUVs need to coordinate their motion to receive energy, maintain wireless network integrity, and accomplish their tasks. It is highly complex to jointly design this system. This paper focuses on developing reliable WC and WET algorithms and optimal motion control policies for mobile chargers and AUVs in a swarm. To the best of our knowledge, this is the first paper investigates the joint design of WC, WET, and motion control for swarm AUVs. Our contributions are summarized as follows.

1) We propose a mobile WET system architecture for swarm AUVs, which jointly considers WC, WET, networking, motion control, and swarm missions. The developed model characterizes the complex interplay among various design aspects. The system has potentials to enable persistent sensing and target tracking and automate complex and dangerous tasks by using tiny cheap AUVs in harsh underwater environments.
2) The success of such a complex system design relies on accurate but simple models. To this end, we develop succinct underwater WC and WET models using tri-axis coils, upon which we obtain the optimal transmission policies. Also, we provide the upper bounds and lower bounds of the communication data rate and received energy. We find that by using Channel State Information (CSI), the WC and WET are not affected by coil orientations. However, due to the high mobility of AUVs, it is not practical for a receiver to feedback CSI to a transmitter and, even if it is possible, the CSI will be out-of-date soon, which cannot be used to create optimal beamforming algorithms. We develop transmission policies without using CSI and show that the performance loss is predictable and controllable.
3) Since the orientation loss can be overcome by using tri-axis coils, we develop a low-complexity MI underwater channel model, which does not involve the effect of coil orientation. The channel model with Bessel functions in [9] requires a huge amount of computation, which cannot provide an effective solution within a limited time. Thus, this is an important step to design the proposed swarm AUVs system due to its low computation weight.
4) We develop swarm AUVs motion control policies by considering the constraints of wireless networking integrity, WET efficiency, and AUVs' tasks. The wireless network integrity needs to be satisfied for localization [3] and swarm dynamics, otherwise, some AUVs may be lost. It is achieved by using a robust routing model and adaptive AUV velocity. Continuous AUV motion control is achieved by using a gradient controller. The proposed solution is analyzed theoretically and numerically.

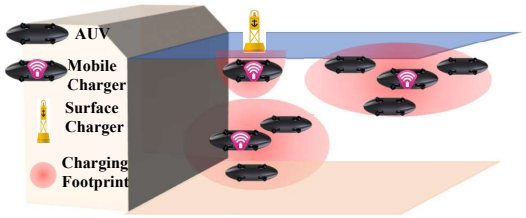

Fig. 1. Illustration of an underwater wireless energy transfer system with a surface charging station and mobile wireless chargers. Mobile chargers are used to wirelessly charge mobile AUVs and they are recharged by surface charging stations.

The rest of this paper is organized as follows. The related works are presented in Section II. In Section III, we provide the system model, and the tri-axis coil-based MI communication and WET model. We develop efficient transmit and receive strategies to optimally use the tri-axis coils for WC and WET. In Section IV, we develop the optimal controllers for AUVs and the mobile charger to maintain network integrity and to improve energy transfer efficiency. After that, in Section V, we present simulation results to show the effectiveness of our approach. Finally, this paper is concluded in Section VI.

II. Related Work

Since the joint design of WC, WET, and motion control for swarm AUVs is novel, which has not been studied in the literature, we provide related works for each individual aspect. MI communication is reliable and power-efficient in underwater environments, which has been tested and proven in [9], [16]. However, applying MI techniques for mobile AUVs faces the following challenges. First, coil misalignment in MI communication can cause significant losses which reduce the effective data transmission rate [17]. For swarm AUVs, the coil misalignment always exists due to AUVs' motion and water turbulence. The tri-axis coil with three mutually perpendicular unidirectional coils can efficiently reduce orientation losses [9], [18]–[20]. Modulation schemes, beamforming algorithms, and channel models have been developed for MI communication with tri-axis coils. Although in [9], [19], it has been proven that the MI communication with tri-axis coils has no orientation loss, the model includes Bessel functions and complex numerical computations, which cannot reveal the fundamental benefits of using tri-axis coils in an intuitive way. Moreover, the developed MI channel model cannot be used for

swarm AUVs due to the prohibitive computation complexity. In this paper, we develop a succinct MI underwater channel model, upon which the gain of using tri-axis coils is obtained analytically in a succinct form. After proving the reliability of tri-axis coils, we simplify the channel model by overcoming the misalignment problem.

Underwater WET provides opportunities to adopt cheaper and smaller AUVs and [12] presents a thorough analysis of its potential applications, technical requirements, and markets. WET in underwater environments experiences more attenuation losses than its counterpart in the air due to the electric conductivity of water. Since our applications are in lakes and rivers, and the attenuation loss is small due to the low conductivity, which reduces the attenuation loss. Moreover, both MI communication and WET use coils, they can share the same tri-axis coil antenna, which can reduce AUV's cost and size. The experiments and simulations in [21], [22] demonstrate the feasibility of underwater WET. Although the charging range is within 1 m, we can improve the distance by increasing the transmission power, as well as the coil size and the number of turns. The prototype built in [23] can successfully recharge static AUVs in underwater and the distance between the transmitter and the receiver is around 1 cm. This technology can be used for WET in the surface station, which recharges static AUVs. The recent study in [24] shows that WET for a mobile receiver is also feasible and there is no obvious loss due to mobility. Although transmission policies are developed for WC and there is no clue how to optimally leverage the tri-axis coil for WET to charge mobile AUVs. In [20] the WET beamforming algorithms are developed for underground sensors with tri-axis coils. However, underground sensors are static and their orientations do not change. In this paper, the orientations of AUVs' coils are random and based on our developed model, we obtain an optimal WET transmission policy that is suitable for swarm AUVs.

Terrestrial robotic networks considering wireless communication or networking constraints have been studied in [25]–[28], where robots move on a 2D plane to accomplish their tasks while satisfying wireless networking constraints. Different from existing works, we consider both WC and WET for AUVs in a 3D underwater space. WC and WET are conducted in different time slots to ensure the high efficiency of WET, which is not the simultaneous wireless information and power transfer [29]. Underwater swarm AUVs has been demonstrated in [30]–[32], whereas the WC and WET are not modeled and optimized. Recently, there are a huge amount of works on networking and path planning for Unmanned Aerial Vehicles (UAVs) [33]–[35] to track targets or improve wireless connectivity. Also, UAV-assisted wireless energy transfer algorithms have been developed for various application scenarios, where UAVs are employed to charge static ground sensors or energy harvesters [36]–[39]. The optimal control of the UAV's trajectory and height can improve charging efficiency. The control and localization accuracy also has significant impacts on charging efficiency and analytical and empirical models have been developed to capture this effect [40], [41]. Different from the aforementioned research, in this paper we assume the accurate location information is available and focus on using a mobile charger to wirelessly charge mobile AUVs (AUVs' locations are changing with time) which can also cooperate with the mobile charger to improve the charging efficiency.

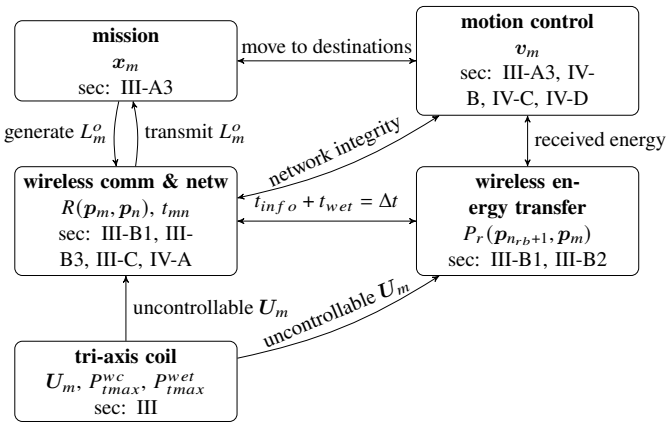

Fig. 2. System overview. The symbols are key parameters of each design component. The *sec:* is the corresponding sections in this paper that cover the design component.

This work is fundamentally different from UAV networks due to the following reasons. First, for AUVs, we use MI communication instead of terrestrial electromagnetic wave-based communications; the communication channels are different. Second, the UAVs' paths are planned ahead and they move following their paths, whereas here we consider the AUVs are autonomous and they move towards their destinations without using predefined paths. Third, the motion of the mobile charger is also jointly designed, which has impacts on swarm AUVs.

III. WC and WET using Tri-axis Coils

In this section, we first introduce the underwater swarm AUVs system model, including communication, networking, WET, and motion control. Then, we identify the key challenges for WC and WET that are caused by motion control. After that, we develop a rigorous analytical model to analyze the WC and WET performance using different antenna systems and obtain the optimal one that can satisfy the requirement of motion control. Finally, we develop a succinct channel model for WC and WET, which can be used to efficiently obtain the optimal motion control policies. An illustration of the system flowchart is given in Fig. 2. A list of symbols and their associated descriptions are given in Table I.

A. Underwater Swarm AUVs System Overview

Assume that there are n_{rb} AUVs in a swarm and a mobile charger which has sufficient energy and computation capability, at locations $\boldsymbol{p}_m = [x_m, y_m, z_m]^T$, for $m = 1, \cdots, n_{rb}, n_{rb}+1$, where the subscript $n_{rb}+1$ represents the mobile charger and $(\cdot)^T$ is the transpose of a vector or a matrix. $\boldsymbol{p}_m(t)$ denotes the location of the mth AUV at time t. In the following, for simplicity, we use $\boldsymbol{p}_m(t)$ and $\boldsymbol{p}_m$ interchangeably without confusion.

1) Wireless Communication and Networking: The mth AUV generates L_m^o bits data periodically, which have information about location, motion, energy, sensing, and wireless network status. Besides sending L_m^o to the destination, an

TABLE I
MATHEMATICAL NOTATION.

Symbol	Description
$\boldsymbol{p}_m$	the mth AUV's location in the 3D underwater environment
n_{rb}	the number of AUVs. The subscription $n_{rb}+1$ stands for the mobile charger
$R(\boldsymbol{p}_m, \boldsymbol{p}_n)$	the achievable communication data rate between the mth AUV at $\boldsymbol{p}_m$ and the nth AUV at $\boldsymbol{p}_n$
t_{mn}	the time that is used by the mth AUV to send data to the nth AUV
t_{info}	the time that can be used for communication in a time slot
t_{wet}	the time that can be used for wireless energy transfer in a time slot
L_m^o	the amount of data that are generated by the mth AUV in a time slot
e_m	a positive number that indicates the ability of the mth AUV to send extra data
$P_r(\boldsymbol{p}_{n_{rb}+1}, \boldsymbol{p}_m)$	the received power by the mth AUV at location $\boldsymbol{p}_m$, the mobile charger's location is $\boldsymbol{p}_{n_{rb}+1}$
E_m^h	the harvested energy by the mth AUV in a time slot
$\boldsymbol{v}_m$	the velocity of the mth AUV
$\boldsymbol{U}_m$	the orientation matrix of a tri-axis coil that is equipped on the mth AUV
$\boldsymbol{u}_{m1}$	the orientation vector of a unidirectional coil in a tri-axis coil
$\boldsymbol{s}_m$	current signals
$\boldsymbol{D}$	the magnetic fields generated by x-, y-, and z-orientated unidirectional coils with unit currents
r_l and r_c	load resistance and coil resistance, respectively
N_c	the coil number of turns
a	the coil radius
ϵ, μ, and σ	perimittivity, permeability, and conductivity, respectively
Δt	the duration of a time slot
α_m	the velocity of the mth AUV
α'_m	the maximum velocity of the mth AUV due to the network integrity constraints
η_1, η_2, and η_3	positive constants used to normalize the task function, network integrity function, and collision avoidance function, respectively
η_4 and η_5	positive constants used to normalize the swarm received power and the individual AUV received power, respectively

AUV may also need to relay packets for other AUVs that cannot directly communicate with their destinations in the swarm. We consider the achievable data rate between the mth AUV and the nth AUV as $R(\boldsymbol{p}_m, \boldsymbol{p}_n)$. The motion of AUVs may change the achievable data rate. In Section IV-C we control the velocity of AUVs to ensure that the data transmission can be successfully accomplished.

We consider that the network can maintain its integrity if all AUVs in a swarm can send out their original and relayed data during the given time t_{info}. A similar approach was used in [25], [26], [42] for terrestrial robotic networks. Network integrity ensures that all the data packets can be sent within given time slots without packet losses due to network congestion. Maintaining network integrity is important for swarm AUVs since AUVs periodically communicate with each other to coordinate their motion. Without network integrity, the swarm AUVs may experience severe network congestion and, even worse, they cannot coordinate with each other to complete their tasks. Let t_{mn} denote the time when AUV m sends data to AUV n. Thus, the data that AUV m can send is $\sum_{n=1,n\neq m}^{n_{rb}+1} t_{mn} R(\boldsymbol{p}_m, \boldsymbol{p}_n)$, and the data that it receives and generates is $\sum_{n=1,n\neq m}^{n_{rb}} t_{nm} R(\boldsymbol{p}_m, \boldsymbol{p}_n) + L_m^o$. The mobile charger is considered as a data sink, which can also collect data from AUVs. It sends negligible amount of data to other AUVs. Also, the mobile charger performs high-cost computing for the AUV swarm. As a result, the network integrity is achieved only if the following condition is satisfied for all the AUVs,

$$L^m(\boldsymbol{p}_m, \boldsymbol{p}_n) - L_m^o \geq e_m, \tag{1}$$

where

$$L^m(\boldsymbol{p}_m, \boldsymbol{p}_n) = \sum_{\substack{n=1 \\ n\neq m}}^{n_{rb}+1} t_{mn} R(\boldsymbol{p}_m, \boldsymbol{p}_n) - \sum_{\substack{n=1 \\ n\neq m}}^{n_{rb}} t_{nm} R(\boldsymbol{p}_m, \boldsymbol{p}_n),$$

and $e_m \geq 0$ is used to adjust the reliability of the network. The above equation is based on that the amount of data that an AUV can send is more than that it received and generated.

2) Wireless Energy Transfer: The mobile charger has sufficient energy to wirelessly charge AUVs. The energy consumption of an AUV is complicated since the motion, sensing, and communication all consume energy which are complex to model considering the dynamic surrounding environment, such as changes of fluid force and depth [43], [44]. In this paper, we model the received energy from the mobile charger. Since the energy consumption is determined by the specific application, we do not consider it here. The harvested energy is $E_m^h(t_n) = \int_{t_{n-1}}^{t_n} P_r(\boldsymbol{p}_{n_{rb}+1}(t), \boldsymbol{p}_m(t))dt$ for $m = 1, \cdots, n_{rb}$, where $P_r(\boldsymbol{p}_{n_{rb}+1}(t), \boldsymbol{p}_m(t))$ is the received power by the mth AUV at time t.

3) Motion: Consider that a swarm of AUVs are tasked to survey multiple points of interest located at $\boldsymbol{x}_m$ for $m = 1, \cdots, n_{rb}$ in underwater. The objective of path planning is to minimize the convex function $\|\boldsymbol{p}_m - \boldsymbol{x}_m\|_2^2$ [26], [42]. In this paper, we assume there is no obstacle and AUVs only need to avoid intra-swarm collisions. The motion of terrestrial robots can be captured by using two degree-of-freedom (DOF) since they move on a horizontal plane [42]. However, the motion of AUVs in the 3D underwater environment is usually modeled using six DOF [45], [46], i.e., pitch, sway, heave, yaw, surge, and roll. In this paper, the location of an AUV is important for WC and WET and the detailed actions that drive AUVs to that location are not considered. Therefore, in this paper, we consider a three-DOF model using AUV locations $\boldsymbol{p}_m$. We consider the system as a simple single input control system $\dot{\boldsymbol{p}}_m = f(\boldsymbol{p}_m, \boldsymbol{v}_m)$, where $\boldsymbol{v}_m$ is the control signal for the mth AUV. The AUVs are fully controllable with simple dynamics and we have $\dot{\boldsymbol{p}}_m = \boldsymbol{v}_m$, for $m = 1, \cdots, n_{rb}$.

4) Joint Design Challenges: First, MI-based comm tion and energy transfer use coils, which have sign power losses if the transmitter and the receiver are no aligned. Thus, when AUVs are moving in underwate need to align their coil orientations to achieve reliable W WET. This can affect their motion continuity, which res inferior swarm performance. Second, as we have show communication data rate $R(\boldsymbol{p}_m, \boldsymbol{p}_n)$ and the AUV re power $P_r(\boldsymbol{p}_{n_{rb}+1}(t), \boldsymbol{p}_m(t))$ are functions of location. fore, the motion control has strong impact on communi data rate and energy transfer efficiency. We cannot let stay close to each other to improve data rate and efficiency since this increases the chance of collision reduces their velocity. Also, the AUV swarm format dynamic due to underwater environmental dynamics. challenging to obtain an optimal formation and let the maintain it. Next, we analyze the WC and WET perfor using tri-axis coils and obtain a low-complexity reliable transmission and reception policy, upon which we devel motion control policy for swarm AUVs in the next sect

B. Modeling and Optimization of WC and WET

MI-based WC and WET suffer from random coil misalignment losses due to the motion of AUVs in the 3D underwater space. By using tri-axis coils with CSI, it is shown in [9], [19] the orientation loss can be minimized to achieve reliable communication. The channel models in [9], [19] are complicated since the coil orientation is considered jointly with magnetic field propagation paths, which makes the relation between the received power and distance untrackable. Thus, we cannot use these models to plan AUVs' motion in this paper. In [8], [10], the coil orientation problem is neglected by optimally deploying coils with predefined orientations, which cannot be used for AUVs. According to [9], [47], underwater magnetic fields propagate to a receiver in three paths, namely, the direct path, the reflected path, and the lateral wave path, as shown in Fig. 3. When the distance from a transmitter to a receiver is small, the direct path is dominant, whereas when the distance is large, the lateral wave is dominant since magnetic fields mainly propagate through the air. Next, we develop the optimal transmit and receive strategies to study the best performance that we can achieve. Here, we compare four configurations, i.e., Single-Input-Single-Output (SISO) using unidirectional coils with random orientations, SISO using unidirectional coils with optimal alignment, Multiple-Input-Multiple-Output (MIMO) using tri-axis coils with random orientations and CSI at the transmitter side, and MIMO using tri-axis coils with random orientations but without CSI at the transmitter side.

In this paper, AUVs and the mobile charger are equipped with tri-axis coils with coil orientation $\boldsymbol{U}_m = [\boldsymbol{u}_{m1}, \boldsymbol{u}_{m2}, \boldsymbol{u}_{m3}]$, for $m = 1, \cdots, n_{rb}+1$, where $\boldsymbol{u} = [x, y, z]^T$ is a unit vector denoting the orientation of a unidirectional coil. Since in the tri-axis coil, orientations of three unidirectional coils are perpendicular to each other, we have $\boldsymbol{u}_m^T \boldsymbol{u}_n = 0$ for $m \neq n$ and $\boldsymbol{U}_m$ is an orthogonal matrix. Let the input current of a tri-axis coil be $\boldsymbol{s}_m = [s_{m1}, s_{m2}, s_{m3}]^T$ for $m = 1, \cdots, n_{rb}+1$. Then, $\boldsymbol{U}_m \boldsymbol{s}_m$ can be considered as the input currents for a regular tri-axis coil with three unidirectional coils pointing to the x, y, and z axes in Cartesian coordinates, respectively [9]. Therefore, although the AUVs may have arbitrarily orientated tri-axis coils, we can project their input currents to a tri-axis coil with regular orientation and study its radiated magnetic fields, which can simplify the analysis.

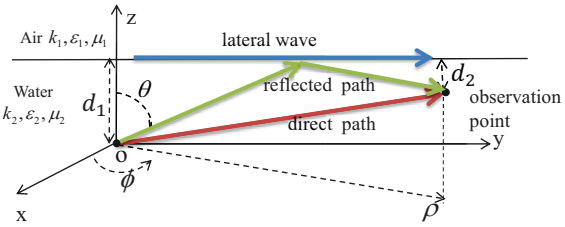

Fig. 3. Cylindrical coordinates for magnetic field propagation in underwater. The transmitter is located at the origin and the receiver is located at the observation point.

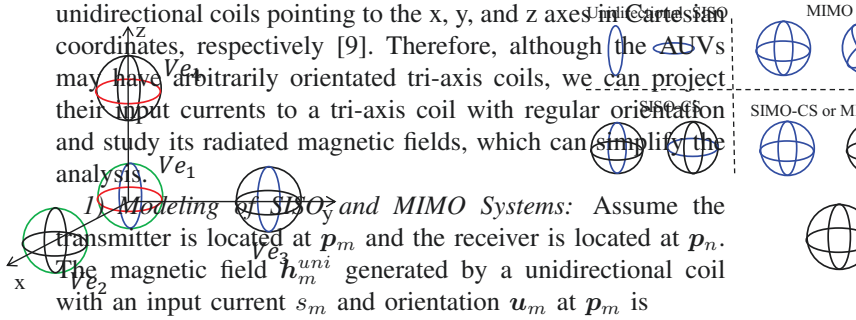

1) Modeling of SISO and MIMO Systems: Assume the transmitter is located at $\boldsymbol{p}_m$ and the receiver is located at $\boldsymbol{p}_n$. The magnetic field $\boldsymbol{h}_m^{uni}$ generated by a unidirectional coil with an input current s_m and orientation $\boldsymbol{u}_m$ at $\boldsymbol{p}_m$ is

$$\boldsymbol{h}_m^{uni} = \begin{bmatrix} h_x \\ h_y \\ h_z \end{bmatrix} = \begin{bmatrix} D_{xx} & D_{yx} & D_{zx} \\ D_{xy} & D_{yy} & D_{zy} \\ D_{xz} & D_{yz} & D_{zz} \end{bmatrix} \begin{bmatrix} u_{mx} \\ u_{my} \\ u_{mz} \end{bmatrix} s_m = \boldsymbol{D}\boldsymbol{u}_m s_m, \tag{2}$$

where $\boldsymbol{D} \in \mathbb{C}^{3\times 3}$ and D_{mn} is the magnetic field in n-direction that is generated by the current component in the transmitting coil in m-direction. s_m is a complex number denoting the transmitted signal. The product of $\boldsymbol{u}_m$ and s_m is equivalent to transmitting signals using three coils with the same orientations as the Cartesian axes, respectively. $\boldsymbol{D}$ is a function of coil configurations and distance, and the detailed formulas are given in Appendix A and [9], [19]. Note that given $\boldsymbol{p}_m$, the receiver location $\boldsymbol{p}_n$, and coil configurations, we can determine the matrix $\boldsymbol{D}$. Here, we do not consider multipath fading effects due to the following two reasons. First, the communication range is within several tens of meters and scattering effects are not strong. Second, the carrier frequency is low, which demonstrates much higher penetration efficiency than terrestrial wideband communications.

The received signal can be expressed in terms of current or voltage. Here, we use voltage signals since they are more succinct and the received signal at the lth symbol interval is

$$y(l) = -j\omega\Lambda_0 \boldsymbol{u}_n^T \boldsymbol{D}\boldsymbol{u}_m s_m(l) + z(l), \tag{3}$$

where $\Lambda_0 = \mu_2 \pi a^2 N_c$ captures the receiving coil configurations, including coil radius a and coil number of turns N_c, and the water permeability μ_2; $j = \sqrt{-1}$, $\omega = 2\pi f_c$, where f_c is the carrier frequency, and $z(l)$ is the complex Gaussian noise. The received power that carries information and energy is

$$P_r^{uni} = \mathop{\mathbb{E}}_{s_m(l)} \left[\frac{\omega^2 s_m^2(l) \Lambda_0^2}{8 r_l} \boldsymbol{u}_m^T \boldsymbol{D}^\dagger \boldsymbol{u}_n \boldsymbol{u}_n^T \boldsymbol{D} \boldsymbol{u}_m \right], \tag{4}$$

where r_l is the load resistance, which is chosen to be equivalent to the coil resistance r_c, and $(\cdot)^\dagger$ is the hermitian of a matrix. In this paper, we use AC resistance and the expression

for r_l can be found in [48]. Note that, the noise power is not considered for WET since it is extremely small. However, in WC we have to consider it, which will be discussed in the communication model.

For the MIMO system using tri-axis coils, the magnetic field at $\boldsymbol{p}_n$ can be written as

$$\boldsymbol{h}^{tri} = \boldsymbol{D}\boldsymbol{U}_m\boldsymbol{s}_m, \tag{5}$$

where $\boldsymbol{s}_m \in \mathbb{C}^{3\times 1}$ is the coil current with modulated information. The received signal at the lth symbol interval is

$$\boldsymbol{y}(l) = -j\omega\Lambda_0\boldsymbol{U}_n^T\boldsymbol{D}\boldsymbol{U}_m\boldsymbol{s}_m(l) + \boldsymbol{z}(l), \tag{6}$$

where $\boldsymbol{y}(l)$, $\boldsymbol{s}_m(l)$, and $\boldsymbol{z}(l)$ are the received signals, transmitted signals, and noises of the tri-axis coil. The received power is

$$P_r^{tri} = \frac{\omega^2\Lambda_0^2}{8r_l}\mathop{\mathbb{E}}_{\boldsymbol{s}_m(l)}\left[tr\left(\boldsymbol{U}_n^T\boldsymbol{D}\boldsymbol{U}_m\boldsymbol{s}_m(l)\boldsymbol{s}_m(l)^\dagger\boldsymbol{U}_m^T\boldsymbol{D}^\dagger\boldsymbol{U}_n\right)\right], \tag{7}$$

where $tr(\cdot)$ is the trace of a matrix. In the above model, we consider that coils have loose coupling since the AUVs cannot be very close to each other to avoid collisions. Thus, the reflected impedance effect that was considered in [49]–[51] is neglected in this paper. We assume that the symbols are i.i.d., i.e., $\mathbb{E}(\boldsymbol{s}_m(l)\boldsymbol{s}_m(l)^\dagger) = \text{diag}(\boldsymbol{\xi})\boldsymbol{I}$, where $\text{diag}(\cdot)$ is a diagonal matrix, $\boldsymbol{\xi}$ is the power allocation vector and $\boldsymbol{I}$ is an identity matrix. Next, we neglect the symbol number l to simplify the notations. The transmission power is $P_t = \mathbb{E}_{s_m}[r_c(s_m)^2]$ for the SISO system, while for the MIMO system we consider the overall transmission power is a constant and it is divided into three portions. WET efficiency highly depends on the received power, while wireless communication is affected by noise, channel bandwidth, and many other factors. Therefore, we need to discuss them individually. In the following, we first study the effect of coil orientation on WET, after which we study its effect on more complicated WC systems.

2) Wireless Energy Transfer: The objective of wireless energy transfer is to maximize the received energy within a limited time slot. In this paper, we assume all the received power can be used to recharge an AUV's battery, i.e., the efficiency is 100%. For a SISO system with random coil orientations, since $\boldsymbol{u}_m$ and $\boldsymbol{u}_n$ are random unit vectors, the received power P_r^{uni} varies significantly. Since $\boldsymbol{u}_n^T\boldsymbol{D}\boldsymbol{u}_m = \|\boldsymbol{u}_n^T\|_2 \cdot \|\boldsymbol{D}\boldsymbol{u}_m\|_2 \cdot \cos\theta$, where θ is the angle between $\boldsymbol{u}_n^T$ and $\boldsymbol{D}\boldsymbol{u}_m$. If $\theta = \pi/2$, $P_r^{uni} = 0$, i.e., the received power is zero and we cannot recharge an AUV. When $\theta = 0$ we obtain the optimal receiving coil orientation $\boldsymbol{u}_n^* = \boldsymbol{D}\boldsymbol{u}_m/\|\boldsymbol{D}\boldsymbol{u}_m\|_2$. The optimal transmitting coil orientation $\boldsymbol{u}_m^*$ is the eigenvector associated with the largest eigenvalue λ_{max1}^2 of $\boldsymbol{D}^\dagger\boldsymbol{D}$ and we can obtain the maximum received power

$$P_r^{uni^*} = \frac{\omega^2\Lambda_0^2 P_{tmax}}{8r_l r_c}\lambda_{max1}^2. \tag{8}$$

As a result, for a SISO system the optimal transmitting and receiving coil orientations are $\boldsymbol{u}_m^*$ and $\boldsymbol{u}_n^*$, respectively. Note that, to obtain the optimal coil orientations, we need the CSI. In free space, when transceivers are close to each other, the optimal orientation is co-axial, which can be derived from transceivers' location. However, the propagation of magnetic fields in the underwater environment is complex due to the existence of lateral waves, which travel along the water-air interface and it is very different from the reflection path or the direct path. Therefore, it is challenging to estimate the optimal orientation $\boldsymbol{u}_m^*$ and $\boldsymbol{u}_n^*$ based on location information.

For a MIMO system using randomly orientated tri-axis coils, we have the following proposition.

Proposition 1. *As a receiving antenna, the tri-axis coil can receive all the available power without any loss caused by the random orientation.*

Proof. Let the magnetic field at $\boldsymbol{p}_n$ be $\boldsymbol{h}^{tri}$, which is given in (5). Now, we use a tri-axis coil with random orientation $\boldsymbol{U}_n = [\boldsymbol{u}_{n1}, \boldsymbol{u}_{n2}, \boldsymbol{u}_{n3}]$ to receive the power that is carried by $\boldsymbol{h}^{tri}$. The received power can be written as

$$P_r^{tri} = \sum_{i=1}^{3}\frac{\omega^2\Lambda_0^2}{8r_l}\boldsymbol{u}_{ni}^T\boldsymbol{h}^{tri}(\boldsymbol{h}^{tri})^\dagger\boldsymbol{u}_{ni} \tag{9}$$

$$= \frac{\omega^2\Lambda_0^2}{8r_l}\left(|\boldsymbol{u}_{n1}^T\boldsymbol{h}^{tri}|^2 + |\boldsymbol{u}_{n2}^T\boldsymbol{h}^{tri}|^2 + |\boldsymbol{u}_{n3}^T\boldsymbol{h}^{tri}|^2\right) \tag{10}$$

$$= \frac{\omega^2\Lambda_0^2}{8r_l}\|\boldsymbol{h}^{tri}\|_2^2. \tag{11}$$

In (9) we use the definition of the received power. In (10), we consider that $\boldsymbol{u}_{n1}$, $\boldsymbol{u}_{n2}$, and $\boldsymbol{u}_{n3}$ are orthonormal basis vectors and they can form a Cartesian coordinates system. Then, $\boldsymbol{h}^{tri}$ is a vector in the system. By projecting $\boldsymbol{h}^{tri}$ onto each axis and norm the coordinates, we have the length of $\boldsymbol{h}^{tri}$ in (11). Therefore, there is no orientation loss at the receiver. □

Up to this point, we have proved that the receiver's orientation does not affect the received power. However, at the transmitter side, the access to CSI and coil orientation information ($\boldsymbol{U}_m$) is important to optimally transmit signals. The motion of an AUV makes it challenging to estimate CSI in a timely manner. Therefore, there is a tradeoff between high energy transfer efficiency and effective motion planning. To compare the energy transfer efficiency with and without CSI and coil orientation information, we give the following proposition.

Proposition 2. *For a MIMO system using tri-axis coils, the maximum received power with transmitter side CSI and $\boldsymbol{U}_m$ is at most 3 times larger than that without transmitter side CSI and $\boldsymbol{U}_m$.*

Proof. First, we derive the maximum received power when the transmitter side CSI and $\boldsymbol{U}_m$ are available. Since there is no misalignment loss at the receiver side, maximizing the received power is equivalent to maximizing $\|\boldsymbol{h}^{tri}\|_2^2$, which is

$$\max_{\boldsymbol{s}_m} \quad \|\boldsymbol{D}\boldsymbol{U}_m\boldsymbol{s}_m\|_2^2 \quad \text{s.t.} \quad \mathbb{E}(tr(r_c\boldsymbol{s}_m\boldsymbol{s}_m^\dagger)) \le P_{tmax}. \tag{12}$$

Let $\boldsymbol{v}_m$ be the right-singular vector associated with the largest eigenvalue λ_{max2}^2 of $\boldsymbol{U}_m^T\boldsymbol{D}^\dagger\boldsymbol{D}\boldsymbol{U}_m$. The solution to the above problem is $\boldsymbol{s}_m = \sqrt{P_{tmax}/r_c}\boldsymbol{v}_m$ and the maximum $\|\boldsymbol{h}^{tri}\|_2^2$ is $\lambda_{max2}^2 P_{tmax}/r_c$. Thus, the maximum received power is

$$P_{r,wi}^{tri^*} = \frac{\omega^2\Lambda_0^2 P_{tmax}}{8r_l r_c}\lambda_{max2}^2. \tag{13}$$

If $\boldsymbol{D}$ and $\boldsymbol{U}_m$ are not available, we cannot solve the problem in (12). In this case, we can equally allocate the transmission power to each coil, i.e., $\mathbb{E}(\boldsymbol{s}_m\boldsymbol{s}_m^\dagger) = P_{tmax}/(3r_c)\boldsymbol{I}$. As a result,

$$\mathbb{E}(\|\boldsymbol{h}^{tri}\|_2^2) = \mathbb{E}(tr(\boldsymbol{D}\boldsymbol{U}_m\boldsymbol{s}_m\mathbf{s}_m^\dagger\mathbf{U}_m^T\mathbf{D}^\dagger)) = \sum_{i=1}^{3}\frac{P_{tmax}}{3r_c}\lambda_i^2, \tag{14}$$

where λ_i^2 is the eigenvalue of $\boldsymbol{U}_m^T\boldsymbol{D}^\dagger\boldsymbol{D}\boldsymbol{U}_m$ and $\max(\lambda_1^2,\lambda_2^2,\lambda_3^2) = \lambda_{max2}^2$. Then, the maximum received power is

$$P_{r,wo}^{tri^*} = \frac{\omega^2\Lambda_0^2 P_{tmax}}{24r_l r_c}\sum_{i=1}^{3}\lambda_i^2. \tag{15}$$

From (13) and (15), we can easily find that

$$P_{r,wo}^{tri^*} \le P_{r,wi}^{tri^*} \le 3P_{r,wo}^{tri^*}. \tag{16}$$

Therefore, the maximum received power with CSI and $\boldsymbol{U}_m$ is at most 3 times larger than that without CSI and $\boldsymbol{U}_m$. □

It is worth noting that although the optimal transmission signal $\boldsymbol{s}_m$ depends on the coil orientation when the CSI and $\boldsymbol{U}_m$ are available, the maximum received power is independent of $\boldsymbol{U}_m$. In other words, given $\boldsymbol{D}$ and different $\boldsymbol{U}_m$, we can always find the optimal $\boldsymbol{s}_m$ to achieve the same maximum received power $P_{r,wi}^{tri^*}$. The underlying reason is due to the following proposition.

Proposition 3. *For a MIMO system using tri-axis coils, the maximum received power is independent of the transmitting coil orientation.*

Proof. Note that both $P_{r,wi}^{tri^*}$ and $P_{r,wo}^{tri^*}$ are functions of the eigenvalues of $\boldsymbol{U}_m^T\boldsymbol{D}^\dagger\boldsymbol{D}\boldsymbol{U}_m$. Next, we prove that the eigenvalues of $\boldsymbol{U}_m^T\boldsymbol{D}^\dagger\boldsymbol{D}\boldsymbol{U}_m$ are the same as the eigenvalues of $\boldsymbol{D}^\dagger\boldsymbol{D}$. First, let $\boldsymbol{D} = \boldsymbol{U}_D\boldsymbol{\Sigma}_D\boldsymbol{V}_D^\dagger$ and $\boldsymbol{U}_m = \boldsymbol{U}_U\boldsymbol{\Sigma}_U\boldsymbol{V}_U^\dagger$ be the singular value decompositions of $\boldsymbol{D}$ and $\boldsymbol{U}_m$, respectively. Since $\boldsymbol{U}_m$ is an orthogonal matrix, $\boldsymbol{\Sigma}_U = \boldsymbol{I}$. Thus, we have

$$\boldsymbol{D}\boldsymbol{U}_m = \boldsymbol{U}_D\boldsymbol{\Sigma}_D\boldsymbol{V}_D^\dagger\boldsymbol{U}_U\boldsymbol{I}\boldsymbol{V}_U^\dagger = \boldsymbol{U}_D\boldsymbol{\Sigma}_D\boldsymbol{V}_{DU}^\dagger, \tag{17}$$

where $\boldsymbol{V}_{DU}^\dagger = \boldsymbol{V}_D^\dagger\boldsymbol{U}_U\boldsymbol{V}_U^\dagger$. As we can see, the singular value $\boldsymbol{\Sigma}_D$ does not change and only right-singular vectors are updated. As a result, the eigenvalues of $\boldsymbol{U}_m^T\boldsymbol{D}^\dagger\boldsymbol{D}\boldsymbol{U}_m$ are the same as that of $\boldsymbol{D}^\dagger\boldsymbol{D}$. As a result, the maximum received power in (13) and (15) are independent of transmitting coil orientation. □

Based on Proposition 1 and Proposition 3, we can draw the conclusion that the received power of using the MIMO system with tri-axis coils is not affected by coil orientations. Also, from Proposition 3 we learn that $\lambda_{max1} = \lambda_{max2}$ and, thus, (8) is equivalent to (13). As a result, the performance of a MIMO system using tri-axis coils with transmitter side CSI has the same received power as a SISO system with optimal coil orientations.

3) Wireless Communication: The objective for wireless communication is to maximize the channel capacity. For a SISO system, the maximum capacity is

$$R_{info}^{uni^*} = B\log_2\left(1+\frac{P_r^{uni^*}}{P_{noise}}\right), \tag{18}$$

where B is the signal bandwidth, $P_{noise} = BN_0$ is the noise power, and $N_0/2$ is the noise power spectra density. The capacity is directly related to the received power. As discussed before, the received power of a SISO system with random coil orientation can vary from 0 to $P_r^{uni^*}$, which is given in (8), while a SISO system with optimal coil orientations can always achieve $P_r^{uni^*}$. Thus, the capacity of a SISO system with random coil orientations varies from 0 to $R_{info}^{uni^*}$, while the capacity of a SISO system with optimal coil orientation is always $R_{info}^{uni^*}$.

For a MIMO system using tri-axis coils, the capacity has been extensively studied in [9], [29], [52], [53]. The optimal capacity is achieved by using spatial multiplexing, which is

$$R_{wi}^{tri*} = B\sum_{i=1}^{3}\log_2\left(1+\frac{\omega^2\Lambda_0^2 P_i}{8r_l r_c P_{noise}}\lambda_i^2\right), \tag{19}$$

where P_i is the allocated transmission power for the ith unidirectional coil based on the water-filling algorithm [54]. When we do not have the knowledge of $\boldsymbol{D}$ and $\boldsymbol{U}_m$, the maximum capacity that can be achieved by equally allocate transmission power, which is

$$R_{wo}^{tri*} = B\sum_{i=1}^{3}\log_2\left(1+\frac{\omega^2\Lambda_0^2 P_{tmax}}{24r_l r_c P_{noise}}\lambda_i^2\right). \tag{20}$$

Note that, both R_{wi}^{tri*} and R_{wo}^{tri*} are also independent of the transmitting and receiving coil orientations. In the high SNR regime, $R_{wo}^{tri*} \approx R_{wi}^{tri*} \approx 3R_{info}^{uni^*}$.

Generally, we have proven that by using a MIMO system we can achieve reliable wireless energy transfer and communication without being affected by coil random orientations. Note that, for a SISO system, to obtain the optimal orientation, an AUV has to move to align coil orientations. For a MIMO system, we do not require coil alignment.

C. A Simplified Underwater Channel Model

Since the received power of a MIMO system is independent of coil orientations, we can develop a simple channel model without random coil orientations, which simply shows the relation between the received power and the AUV distance. This can be used to efficiently develop motion control algorithms to maintain wireless connectivity within a swarm and achieve high WET efficiency.

The underwater wireless communication channel model using magnetic induction was developed in [8], [10] for the deep underwater environment without considering the water-air interface. In [9], the effect of the water-air interface was considered and a rigorous channel model was developed by solving Maxwell's equations. Since we consider that AUVs are in shallow low-conductive water, the model in [9] is more related to this paper. However, the relation between the AUV

distance and the received power involves Bessel functions, which cannot be used to develop an effective motion algorithm for swarm AUVs.

The received power using a MIMO system can be bounded by that of using a SISO system with optimal coil orientation, as shown in equations (8), (13), (15), and (16). Therefore, we can develop a channel model for the SISO system with optimal coil orientations then obtain the relation between the developed model with the channel model of a MIMO system. In this way, we can simplify the magnetic field vector additions as well as the effect of random coil orientation.

The results in [9], [47] show that there are primarily three magnetic field propagation paths, namely, the direct path, reflected path, and lateral waves traveling in the air, which are shown in Fig. 3, where d_1 and d_2 are the depth of the transmitter and receiver, respectively, and ρ is their horizontal distance. The direct path and the reflected path are in the water. First, when $d_1 + d_2 > \rho$, the lateral wave can be neglected since signals experience more attenuation losses propagating to the surface to generate lateral waves. Compared with the direct path, the reflected path is longer and attenuated by reflections on the boundary. Thus, reflected signals are weaker than signals propagating along the direct path. Also, since the baseband signal bandwidth is small and the carrier frequency is low, reflected signals are unresolvable and their delay can be neglected. Based on these reasons, we can neglect the reflected path. Second, the lateral wave can be dominant when the distance between the transmitter and the receiver is much larger than their depth, where signals experience significant losses in the direct path. Next, we analyze the direct path and the lateral wave and develop a simple model to capture the dominant factors for the underwater MI communication channel.

1) Direct Path: The dominant magnetic fields for the direct path can be written as

$$\boldsymbol{h}^{dir} = \begin{bmatrix} h_r \\ h_\theta \\ h_\phi \end{bmatrix} = \left[\frac{a^2 N_c s}{2r^3} e^{jk_2 r}, \frac{-k_2^2 a^2 N_c s}{4r} e^{jk_2 r}, 0 \right]^T, \quad (21)$$

where s is the input current, $r = \|\boldsymbol{p}_m - \boldsymbol{p}_n\|_2$ is the distance between the mth and the nth AUV, $k_2 = \omega\sqrt{\epsilon_2 \mu_2}$, $\epsilon_2 = \epsilon_w + j\sigma/\omega$, and ϵ_w, σ, and μ_2 are the water permittivity, conductivity, and permeability, respectively. The detailed derivations are given in Appendix B. By using the tri-axis receiver we can receive all the power carried by $\boldsymbol{h}^{dir}$, which is

$$P_r^{dir} = \frac{\omega^2 \Lambda_0^2}{8 r_l} \boldsymbol{h}^{dir\dagger} \boldsymbol{h}^{dir} \quad (22)$$

$$= \frac{\omega^2 \Lambda_1^2 P_{tmax}}{32 r_l r_c} \left(r^{-6} + \frac{|k_2|^4}{4} r^{-2} \right) e^{-2k_2^{im} r} \quad (23)$$

where $\Lambda_1 = \mu_2 \pi a^4 N_c^2$ and $k_2^{im} = \Im(k_2)$, which is the imaginary part of k_2.

2) Lateral Wave: The dominant magnetic fields for the lateral wave can be written as

$$\boldsymbol{h}^{la} = \begin{bmatrix} h_\rho \\ h_\phi \\ h_z \end{bmatrix} = \frac{-jsN_c a^2 k_1^2}{2k_2 r^2} e^{jk_2(d_1+d_2)+jk_1 r} [\frac{k_2}{k_1}, \frac{jk_2}{k_1^2 r}, 0]^T \quad (24)$$

where $k_1 = \omega\sqrt{\epsilon_1 \mu_1}$ and ϵ_1 and μ_1 are the air permittivity and permeability, respectively. Note that, the lateral wave is dominant only if r is much larger than d_1 and d_2 and, thus, r can be used to approximate the horizontal distance. The received power is

$$P_r^{la} = \frac{\omega^2 \Lambda_0^2}{8 r_l} \boldsymbol{h}^{la\dagger} \boldsymbol{h}^{la} \quad (25)$$

$$= \frac{\omega^2 \Lambda_1^2 k_1^2 P_{tmax}}{32 r_l r_c} \left(r^{-4} + \frac{1}{k_1^2} r^{-6} \right) e^{-2k_2^{im}(d_1+d_2)}. \quad (26)$$

Note that $d_1 + d_2$ can be rewritten as $2d_1 - \boldsymbol{p}_n(3)$, where $\boldsymbol{p}_n(3)$ is the z-coordinate of the receiving AUV.

As a result, the overall received power is $P_r = P_r^{dir} + P_r^{la}$. It should be noted that the phases of the direct path and the lateral wave may not be aligned. When we add them together, the phase misalignment may reduce the received power. However, as discussed in [9], [47], the direct path and the lateral wave play dominant roles at different distances. If one is strong, the other one is weak. As a result, we can add the received power without considering the phase misalignment. Also, the Doppler fading can be neglected since the AUV's velocity is small.

To achieve the maximum received power and channel capacity, a MIMO system using tri-axis coils requires CSI. However, the CSI becomes out-of-date quickly due to the motion of AUVs and underwater dynamics. The cost of channel estimation is high which involves communications and signal processing. To reduce the complexity of the system and increase its robustness, we consider the AUVs using the MIMO system without CSI, i.e., the transmission power is equally allocated to coils. In this way, we do not require channel estimation, which can reduce communication overhead and simplify AUVs motion planning. Thus, the achievable data rate is $R(\boldsymbol{p}_m, \boldsymbol{p}_n) = R_{wo}^{tri*}$. As discussed in preceding sections, without CSI the received power is at least 1/3 of the optimal value and we have $P_r(\boldsymbol{p}_{n_{rb}+1}(t), \boldsymbol{p}_m(t)) \geq 1/3 P_r^{uni^*} = 1/3 P_{r,wi}^{tri^*}$, where the optimal values are obtained by using the distance $\|\boldsymbol{p}_m(t) - \boldsymbol{p}_{n_{rb}+1}(t)\|_2$. In the next section, we provide communication and WET performance analysis based on this power allocation approach. Also, when an AUV is communicating with another AUV, it may lose connectivity soon due to its motion. This problem will be addressed in the next section, where WC, WET, and AUV motion will be designed jointly.

IV. Motion Control of Swarm AUVs

In this section, we consider all the AUVs as well as the mobile charger to be equipped with tri-axis coils without CSI for WC and WET. First, we obtain the optimal networking parameters to satisfy network integrity requirements. After that, we develop optimal controllers for AUVs and the mobile charger. Lastly, we evaluate the effect of motion on network integrity and WET.

A. Optimal Parameters for Network Integrity

Based on preceding discussions we learn that the swarm AUVs has multiple objectives. It has to maximize WET efficiency, move towards their destinations, and maintain network

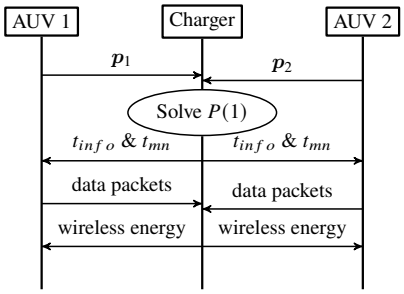

Fig. 4. Underwater mobile wireless charging protocol for swarm AUVs. As an example, the AUV number is 2 in this figure.

integrity. Existing robot path planning algorithms considering wireless communication usually divide the continuous-time into discrete time slots and then optimize the system [27], [35], where only one robot is used. If we adopt this approach for a swarm of AUVs, we have to solve a complicated optimization problem for each AUV during each short time slot, which incurs significant computation burden and communication overhead.

In this paper, we employ the continuous-time motion gradient control along with a discrete-time communication protocol [25]. Different from [25], which tries to maximize the network throughput and increase network routing robustness, we pay special attention to network integrity and AUVs' WET efficiency. Consider the time of a discrete step as $\Delta t = t_{info} + t_{wet}$, where t_{info} is the time used for WC and t_{wet} is the time used for WET. AUVs send data during t_{info} and we assume they have perfect scheduling without interference and collisions. During t_{wet}, the mobile charger broadcasts WET signals using high transmission power and WC cannot be conducted during this time. A protocol is shown in Fig. 4. Then, we have the following problem,

$$\begin{aligned} P(1): \quad & \min_{t_{info}, t_{mn}} t_{info}^2 + \sum_{n=1}^{n_{rb}+1} \sum_{m=1}^{n_{rb}+1} (t_{mn}^2) \qquad (27) \\ & s.t.\ (1); t_{mn} \geq 0, \forall\ t_{mn};\ 0 < t_{info} \leq \Delta t; \\ & \sum_{\substack{n=1 \\ n \neq m}}^{n_{rb}+1} t_{mn} + \sum_{\substack{n=1 \\ n \neq m}}^{n_{rb}} t_{nm} \leq t_{info}, \forall\ m \leq n_{rb}; \\ & \sum_{m=1}^{n_{rb}} t_{mn_{rb+1}} \leq t_{info}; t_{n_{rb+1}m} = 0, \forall\ m. \end{aligned}$$

The objective function (27) consists of two parts. We minimize the first term in order to increase the time for WET since Δt is a constant. We minimize the second term in order to distribute the network traffic to more paths to improve routing reliability [25]. In this way, we can improve the received energy by using the minimum time to transmit data and saving more time for WET.

The above problem can be solved efficiently using existing convex optimization tool CVX [55]. In [25], the robotic network employs distributed algorithms to find the optimal networking parameters t_{mn}. However, since we have a powerful mobile wireless charger, which can provide energy as well as high-performance computing, it can be used to find globally optimal solutions to $P(1)$. The mobile charger requires information about AUVs' locations to plan its motion to charge them. This information can also be leveraged to solve the problem $P(1)$. First, mobile charger collects AUVs locations. Then, it solves problem $P(1)$ and broadcasts the updated parameters to AUVs. One may argue that the scalability of the solution is limited. However, note that a mobile charger is not expected to charge a large scale AUV network. It can only charge a limited number of AUVs. For a large scale AUV network, multiple mobile chargers can be employed and they have to allocate tasks and align their signals.

B. AUV Motion Controller

In this paper, we adopt a continuous motion control algorithm by using a gradient controller. Next, we develop navigation potential functions inspired by [25], [26], [56] and the AUVs are *point robots* [25], [28], [42], [56]. First, to accomplish the mth AUV's task, we need to minimize the following function

$$f_1(\boldsymbol{p}_m) = \frac{\|\boldsymbol{p}_m - \boldsymbol{x}_m\|_2^2}{\eta_1 + \|\boldsymbol{p}_m - \boldsymbol{x}_m\|_2^2}, \qquad (28)$$

where η_1 is a positive constant. The above equation is defined to normalize its value to $[0, 1)$. Since the design takes into account various aspects with different units and ranges of value, jointly optimizing them is not trivial. The results may be affected by one component with extreme values. By using the above function, we can normalize all of them to the same range. For example, by using $f_1(\boldsymbol{p}_m)$ we can normalize the distance to destination. To guarantee network integrity, the data traffic of the mth AUV is

$$f_2(\boldsymbol{p}_m) = \frac{L^m(\boldsymbol{p}_m, \boldsymbol{p}_n) - L_m^o - e_m}{\eta_2 + L^m(\boldsymbol{p}_m, \boldsymbol{p}_n) - L_m^o - e_m}, \qquad (29)$$

where η_2 is a positive constant to normalize the network integrity. A large $f_2(\boldsymbol{p}_m)$ can ensure network integrity. To avoid intra-swarm collisions, the distance between two AUVs has to be monitored. Since the communication signal is directly related to AUVs' distances, the AUV m only evaluates the distance between itself and its communication neighbors. Also, the distance information can be directly transmitted through the wireless network without using relays. Thus, the potential function to avoid collisions is

$$f_3(\boldsymbol{p}_m) = \prod_{n \in \mathcal{P}_m} \frac{\|\boldsymbol{p}_m - \boldsymbol{p}_n\|_2^2}{\eta_3 + \|\boldsymbol{p}_m - \boldsymbol{p}_n\|_2^2}, \qquad (30)$$

where $\mathcal{P}_m$ includes all the AUVs that are neighbors of the AUV m in the network, and η_3 is a positive scalar to adjust the effect of AUV distances. When there is a collision, $f_3(\boldsymbol{p}_m) = 0$. When the distance between AUVs are large, $f_3(\boldsymbol{p}_m) \approx 1$. The navigation function strives to maximize $f_3(\boldsymbol{p}_m)$.

In this paper, we consider two policies for WET:

- Policy 1: WET is a service and the mobile charger does not interrupt the AUVs, i.e., AUVs do not cooperate to improve WET efficiency.
- Policy 2: AUVs move cooperatively with the mobile charger to maintain high WET efficiency.

In the first case, the AUVs' navigation potential function is

$$\phi_m^{rb1} = \frac{f_1(\boldsymbol{p}_m)}{[f_1(\boldsymbol{p}_m)^k + f_2(\boldsymbol{p}_m)f_3(\boldsymbol{p}_m)]^{\frac{1}{k}}}, \tag{31}$$

where k is a positive constant, and the velocity is $\boldsymbol{v}_m = -\alpha_m \nabla_{\boldsymbol{p}_m} \phi_m^{rb1} / \|\nabla_{\boldsymbol{p}_m} \phi_m^{rb1}\|_2$. where α_m is a positive number which scales AUVs' velocity. As shown in [56], the potential function is defined in this way to avoid infinitely large robot velocity and satisfy the preceding requirements. The mobile charger aims to provide the maximized energy to AUVs. During the time slot t_{wet}, it is challenging to update AUVs' location in real-time. The mobile charger uses the location information that are collected during t_{info} to create the following potential function

$$f_4(\boldsymbol{p}_{n_{rb}+1}) = \frac{\sum_{n\in\mathcal{B}} P_r(\boldsymbol{p}_{n_{rb}+1}, \boldsymbol{p}_n)}{\eta_4 + \sum_{n\in\mathcal{B}} P_r(\boldsymbol{p}_{n_{rb}+1}, \boldsymbol{p}_n)}, \tag{32}$$

where $\mathcal{B}$ is the set of AUVs that need to be charged and η_4 is a scalar to normalized the overall received power. The mobile charger takes into account the overall received power by the AUV swarm. Due to the limited space, we do not consider fairness here. If an AUV's battery is higher than a threshold, it is removed from $\mathcal{B}$. Then, the navigation potential for the mobile charger is

$$\phi^{mc} = \frac{1}{[1 + f_2(\boldsymbol{p}_{n_{rb}+1}) f_3(\boldsymbol{p}_{n_{rb}+1}) f_4(\boldsymbol{p}_{n_{rb}+1})]^{\frac{1}{k}}}. \tag{33}$$

The mobile charger does not have a destination and thus its $f_1(\boldsymbol{p}_{n_{rb}+1}) = 1$. Its velocity can be obtained by using $\boldsymbol{v}_{n_{rb}+1} = -\alpha_{n_{rb}+1} \nabla_{\boldsymbol{p}_{n_{rb}+1}} \phi^{mc} / \|\nabla_{\boldsymbol{p}_{n_{rb}+1}} \phi^{mc}\|_2$, where $\alpha_{n_{rb}+1}$ is a positive number that scales the mobile charger's velocity.

In the first case, AUVs are mission-driven and cannot cooperate with the mobile charger. In the second case, AUVs navigate to their destinations and can adjust their path to improve WET efficiency. For the mth AUV, the WET potential is

$$f_5(\boldsymbol{p}_m) = \frac{P_r(\boldsymbol{p}_{n_{rb}+1}, \boldsymbol{p}_m)}{\eta_5 + P_r(\boldsymbol{p}_{n_{rb}+1}, \boldsymbol{p}_m)}, \tag{34}$$

where η_5 is a positive scalar, and its potential function is updated as

$$\phi_m^{rb2} = \frac{f_1(\boldsymbol{p}_m)}{[f_1(\boldsymbol{p}_m)^k + f_2(\boldsymbol{p}_m) f_3(\boldsymbol{p}_m) f_5(\boldsymbol{p}_m)]^{\frac{1}{k}}}. \tag{35}$$

An AUV moves to the location that can improve its received power from the mobile charger while it is moving towards its destination. The mobile charger's potential function does not change. The velocity of AUVs and the mobile charger can be obtained in the same way as that in the first case.

C. Effect of Mobility on Network Integrity

The network parameters are updated every Δt. If Δt is small, significant computations and communication overhead are incurred, while if Δt is large the network information is outdated and the motion of AUVs may violate network integrity, create collisions, and reduce WET efficiency. After the mobile charger updates the networking parameters based on AUVs' locations, AUVs move based on their individual navigation functions without communicating with each other. Therefore, we need to ensure that after Δt the network integrity is still maintained. This is achieved by controlling the AUVs' velocity.

At time t, if all the AUVs can satisfy (1), then to maintain network integrity at time $t + \Delta t$ we need

$$\sum_{\substack{n=1 \\ n\neq m}}^{n_{rb}+1} t_{mn} R'(\boldsymbol{p}_m, \boldsymbol{p}_n) - \sum_{\substack{n=1 \\ n\neq m}}^{n_{rb}} t_{nm} R'(\boldsymbol{p}_m, \boldsymbol{p}_n) - L_m^o \geq 0, \tag{36}$$

where $R'(\boldsymbol{p}_m, \boldsymbol{p}_n)$ is the data rate between AUV m and AUV n at $t + \Delta t$. According to [25],

$$|R'(\boldsymbol{p}_m, \boldsymbol{p}_n) - R(\boldsymbol{p}_m, \boldsymbol{p}_n)| \leq \int_t^{t+\Delta t} |\dot{R}(\boldsymbol{p}_m(\tau), \boldsymbol{p}_n(\tau))| d\tau, \tag{37}$$

where $\dot{R}(\boldsymbol{p}_m(\tau), \boldsymbol{p}_n(\tau))$ is the derivative of $R(\boldsymbol{p}_m, \boldsymbol{p}_n)$ and $\boldsymbol{p}_m(\tau)$ is the location of AUV m at time τ. Then, we have

$$\begin{aligned}
|\dot{R}(\boldsymbol{p}_m, \boldsymbol{p}_n)| &= \left| \frac{dR(\boldsymbol{p}_m, \boldsymbol{p}_n)}{d\|\boldsymbol{r}_{mn}\|_2} \frac{d}{dt} \|\boldsymbol{r}_{mn}\|_2 \right| \\
&= \left| \frac{dR(\boldsymbol{p}_m, \boldsymbol{p}_n)}{d\|\boldsymbol{r}_{mn}\|_2} \frac{(\boldsymbol{r}_{mn})^T}{\|\boldsymbol{r}_{mn}\|_2} \left(\frac{-\alpha_m \nabla_{\boldsymbol{p}_m} \phi_m^{rb1}}{\|\nabla_{\boldsymbol{p}_m} \phi_m^{rb1}\|_2} + \frac{\alpha_n \nabla_{\boldsymbol{p}_n} \phi_n^{rb1}}{\|\nabla_{\boldsymbol{p}_n} \phi_n^{rb1}\|_2} \right) \right| \\
&\leq \left| \frac{dR(\boldsymbol{p}_m, \boldsymbol{p}_n)}{d\|\boldsymbol{r}_{mn}\|_2} \right| (\alpha_m + \alpha_n) \leq 2\alpha'_m \left| \frac{dR(\boldsymbol{p}_m, \boldsymbol{p}_n)}{d\|\boldsymbol{r}_{mn}\|_2} \right|,
\end{aligned} \tag{38}$$

where $\boldsymbol{r}_{mn} = \boldsymbol{p}_m - \boldsymbol{p}_n$, α'_m is the maximum AUV velocity for AUV m and its neighbors and $\left| \frac{dR(\boldsymbol{p}_m, \boldsymbol{p}_n)}{d\|\boldsymbol{r}_{mn}\|_2} \right|$ can be obtained by using (18). Next, we define $\Delta R = \max_{\boldsymbol{p}_n} 2\alpha'_m \Delta t \left| \frac{dR(\boldsymbol{p}_m, \boldsymbol{p}_n)}{d\|\boldsymbol{d}_{mn}\|_2} \right|$. Then, in the worst case the first two terms in (36) can be updated as

$$\begin{aligned}
&\sum_{\substack{n=1 \\ n\neq m}}^{n_{rb}+1} t_{mn} \left[R(\boldsymbol{p}_m, \boldsymbol{p}_n) - \Delta R \right] - \sum_{\substack{n=1 \\ n\neq m}}^{n_{rb}} t_{nm} \left[R(\boldsymbol{p}_m, \boldsymbol{p}_n) + \Delta R \right] \\
&\geq -\Delta R t_{info} + e_m + L_m^o.
\end{aligned} \tag{39}$$

Therefore, in the worst case (36) can be simplified to $-\Delta R t_{info} + e_m \geq 0$ and thus

$$\alpha'_m \leq \frac{e_m}{2 t_{info} \Delta t} \frac{1}{\left| \frac{dR(\boldsymbol{p}_m, \boldsymbol{p}_n)}{d\|\boldsymbol{r}_{mn}\|_2} \right|}. \tag{40}$$

From the above equation, we learn that if t_{info} is large, which means the AUV network spends long time to send current data packets to their destinations, AUVs have to move slowly, otherwise before data packets are sent, the network status has changed significantly and data transmission through the network becomes unreliable. When Δt is small, the network parameters are updated frequently and, thus, AUVs can move fast. On the contrary, when Δt is large, the network parameters are updated slowly and AUVs have to move slowly to maintain network integrity. Also, the AUVs' maximum velocity is modulated by the data transmission capacity. If the network can accommodate more data transmission, i.e., a large e_m, AUVs can move faster, while if e_m is small, which means

the network is on the boundary of violating network integrity, AUVs have to move slowly so that they can check network status frequently. At time $t+\Delta t$, the AUV re-evaluates its e_m and updates the maximum velocity. In addition, an optimal initialization is necessary, i.e., when the AUVs start to move at $t = 0$, their locations have to satisfy network integrity requirements. Also, the AUV has a speed limit v_{max} which is defined
of an A

D. Effe

The r
Since th
is chang
to obtai
end, we
received
is E_m^h
the abov

$$E_m^h$$

where
$P_r(\boldsymbol{p}_{n_{rb}}$
Similar

Then, we define $\Delta P_r = 2\alpha'_m t_{wet} \left| \frac{d\Gamma_r(\boldsymbol{p}_m, \boldsymbol{p}_n)}{d\|\boldsymbol{r}_{mn}\|_2} \right|$. Next, we have

$$E_m^h \leq t_{wet} \left[P_r(\boldsymbol{p}_{n_{rb}+1}(t), \boldsymbol{p}_m(t)) + \Delta P_r \right], \tag{43}$$

and

$$E_m^h \geq t_{wet} \left[P_r(\boldsymbol{p}_{n_{rb}+1}(t), \boldsymbol{p}_m(t)) - \Delta P_r \right], \tag{44}$$

which are the upper bound and lower bound of the received energy of AUV m, respectively. In view of (43) and (44), if the AUV velocity is zero, the upper bound and the lower bound are equivalent. This indicates that the uncertainty of the amount of received energy is caused by the AUV's mobility. Also, the AUV and the mobile charger with nonzero velocity may move towards each other to increase the received energy, or they may move away from each other and the received energy decreases.

V. Performance Evaluation

In this section, we evaluate the proposed underwater MI channel model for tri-axis coils, as well as the mobile WET policies for swarm AUVs.

A. Reliable WET and WC using Tri-axis Coils

The received power models in Section III-B assume the distance between the robots is far enough to neglect near field effects. However, the distance between the two robots may be small when they are moving. In this case, the received power is larger than the transmission power, which cannot be true. To consider the strong coupling in the near field, we consider

TABLE II
Simulation parameters.

Symbol	Value	Symbol	Value	Symbol	Value
a	0.15 m	N_c	50	L_m^o	10 kb
Δt	5 s	P_{tmax}^{wc}	10 dBm	P_{tmax}^{wet}	500 W
η_1	10^4	η_2	1	η_3	0.001
η_4	0.01	η_5	0.005	v_{max}	1 m/s

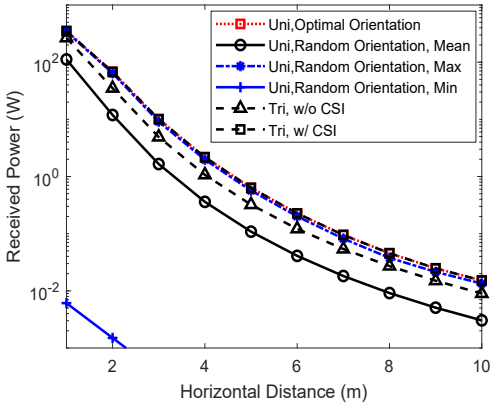

Fig. 5. Received power of using unidirectional coil with optimal orientation, unidirectional coil with random orientation, tri-axis coil with water filling algorithm, and tri-axis coil without water filling algorithm.

the received power as $P_r^g = \frac{P_r}{P_{tmax}+P_r} P_{tmax}$, where P_r is the received power models in Section III-B, including (4), (7), (8), (13), and (15). In this way, we can ensure that when the coil coupling is strong, we can achieve around 100% efficiency but no more than that.

The simulation parameters are given in Table II, where P_t^{wc} and P_t^{wet} are the transmission power for WC and WET, respectively. The coils' copper wire radius is 0.5 mm. We consider the depth of the transmitter and the receiver are 2 m and 1 m, respectively. In Fig. 5, we randomly generate coil orientations using the approach in [9] for 1000 times. As we can see, by using unidirectional coils, the maximum received power is much larger than the minimum received power. The minimum received power is extremely small even when the distance between the transmitter and the receiver is small. Also, as predicted by the analytical model the maximum received power of using unidirectional coil is the same as the received power of using optimally orientated unidirectional coils and the tri-axis coils with CSI. The gap between the received power of using tri-axis coils without CSI and that of using tri-axis coils with CSI is smaller than 3 times.

In Fig. 6, we show the wireless channel capacity using (18), (19), and (20). To better show the worst and best cases, we use the minimum and maximum capacity for the unidirectional coils with random orientations. The transmission power is fixed and we gradually increase the noise power to change the SNR. The noise can come from thermal noise in wireless radios or interference. The horizontal distance between the transmitter and the receiver is 20 m. Similarly, we randomly generate coil orientations for 1000 times. As shown in the figure, using unidirectional coils is very unreliable since the difference between the maximum and the minimum capacity

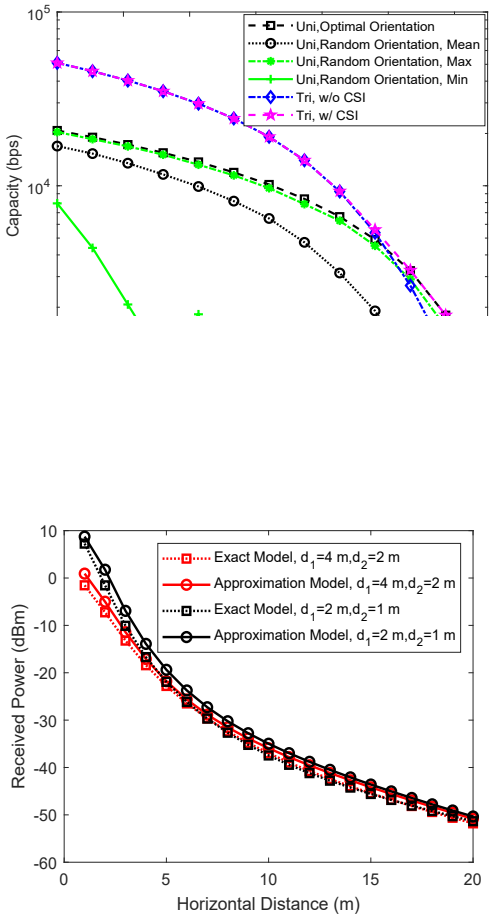

Fig. 7. Comparison of the exact received power model and the approximated received power model.

is very large. When noise power is small, using tri-axis coils with and without CSI have the same performance since the optimal strategy is equally allocating power to each coil. The maximum capacity of using the unidirectional coil with random orientation and the capacity of using an optimally orientated unidirectional coil are about 3 times smaller than that using tri-axis coils. This is due to the multiplexing gain that is offered by a MIMO system. When the noise power is high, the gain disappears and the optimal transmission strategy is to allocate power to the optimally orientated unidirectional coil. Thus, the capacity of using tri-axis coils without CSI achieves lower capacity. The reliability of the tri-axis coil without channel estimation was verified by experiments in [57]; the orientation loss due to misalignment can be efficiently reduced.

In Fig. 7, we compare the simplified received power model in Section III-C with the exact model that is developed in [9] by considering two different transceiver depth. The transmission power is P_t^{wc}. As shown in the figure, when the depth is comparable to their distance, the received power of the shallower case is higher than the deeper case since the direct path is shorter. However, as the distance increases, the two cases converge to the same received power. This is due to the lateral wave, which is dominant when the distance between the transceivers is large. Compared with the exact model, the simplified model is accurate enough and it can provide a simple formula to relate the distance and the received power.

B. Motion Control of Swarm AUVs

In this subsection, we evaluate the developed motion policies for swarm AUVs. We use time-driven simulations in MATLAB. In each time slot, AUVs and the mobile charger update their location, communication, and motion information. We consider there are four AUVs in the swarm and there is one mobile charger. The initial locations of the AUVs and the mobile charger are defined as follows. $\boldsymbol{p}_i = [i, 0, -1]^T$ for $i = 1, \cdots, 5$, where the fifth is the mobile charger. Here, we consider that the AUVs do not change their depth to illustrate their path better. The AUVs are connected if their communication link can support a 10 kbps data rate. Particularly, we consider the following two cases:

1) Case 1: Destinations are distributed uniformly, i.e., $\boldsymbol{x}_i = [i, 50, -1]^T$ for $i = 1, \cdots, 4$, with Policy 1 and Policy 2. Note that, the mobile charger does not have a destination.
2) Case 2: Destinations are distributed randomly, i.e., $\boldsymbol{x}_i = [10 + i + n_d, 50, -1]^T$ for $i = 1, \cdots, 4$, where $n_d \in \mathcal{N}(0, 1)$, with Policy 1 and Policy 2. Here, we shift the destination in the x-direction by 10 m to show the AUVs' ability to adjust their motion towards their destinations.

Note that, we only consider AUVs for about 100 m since the longer path can be divided into multiple short segments using algorithms such as RRT (Rapidly Exploring Random Tree) [58]. Here, we do not consider the energy consumption of AUVs since this is determined by specific tasks that are performed by the AUVs.

In Fig. 8, we show the trajectory of AUVs and the mobile charger using different policies with different destinations. From the figure, we can see that both policy 1 and policy 2 can guide the AUVs to their destinations. In Fig. 8a, the mobile charger first moves towards the AUVs, then it gradually moves a little behind the middle of the swarm to wirelessly charge AUVs. Also, AUVs try to stay away from each other to avoid collisions. In Fig. 8b, the mobile charger stays behind an AUV in the middle of the swarm. Note that, in policy 1, AUVs do not consider their WET efficiency. In Fig. 8c and Fig. 8d, AUVs have to move to improve their WET efficiency while they are moving towards their destinations. In the beginning, AUVs move towards the mobile charger to improve their WET efficiency and the mobile charger chases AUVs to find an optimal position to charge the whole swarm. Thus, they are striving to find a balance. Also, AUVs and the mobile charger moves closer than that using policy 1 since in this way the WET efficiency can be improved. There is a trade-off between avoiding collisions and improving WET efficiency, which can be adjusted by the constants η_3, η_4, and η_5.

In Fig. 9, we show the received energy by each AUV during the simulations. We notice that ΔP_r in (43) and (44) is very small and the bounds are tight. Thus, we use $t_{wet} P_r(\boldsymbol{p}_{n_{rb}+1}(t), \boldsymbol{p}_m(t))$ to estimate the received energy during one Δt. As we can see, by using policy 2 the received energy of each AUV is much higher than that using policy 1.

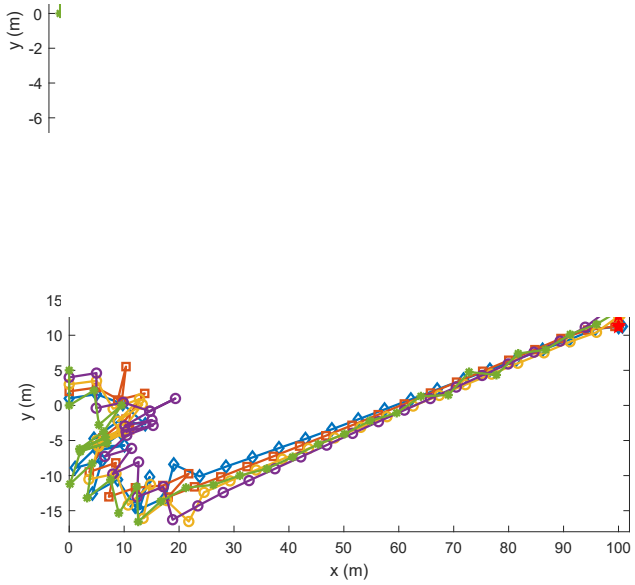

(d) Policy 2, case 2

Fig. 8. Paths of AUVs and the mobile charger using policy 1 and policy 2 with different destinations. The red stars are the destinations of AUVs.

This is because AUVs cooperate with the mobile charger to improve WET efficiency. The state of the art AUV consumes around 10 J energy per second, which is smaller than AUVs' received energy using policy 2. The received energy is sufficient to recharge AUVs. Next, we define the effective velocity as the distance between an AUV's initial location and its destination divided by the time it spends to travel. From Fig. 10 we see that the effective velocity of using policy 2 is much smaller than that of using policy 1. This is because AUVs have to adjust their location to receive more energy which takes more time. Thus, if AUVs' task requires a large velocity, we can use policy 1, otherwise, we can adopt policy 2. There exists a tradeoff between the delay and charging efficiency. If AUVs can maneuver themselves to find the

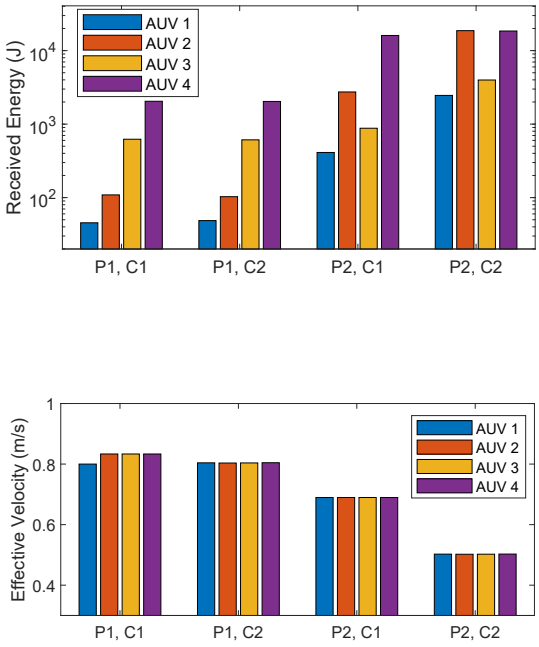

Fig. 10. Effective velocity of AUVs using Policy 1 in Case 1 (P1, C1), Policy 1 in Case 2 (P1, C2), Policy 2 in Case 1 (P1, C1), and Policy 2 in Case 2 (P2, C2).

optimal charging locations, the efficiency can be significantly improved. However, this increases the delay to accomplish their missions. Also, although it is not shown here, the network integrity is always guaranteed during our simulations which is achieved by successfully solving the optimization problem P(1).

In Fig. 11 and Fig. 12 we show the impact of η_3 in (30), which affects the collision avoidance performance, on the distance between two AUVs and received energy. We only show Policy 1 in Case 1 (P1, C1) and Policy 2 in Case 1 (P2, C1) since the performances in Case 2 are similar which do not affect the conclusions. As we can see from Fig. 11, for 4 AUVs and 1 mobile charger, from their initial locations to their destinations, the mean distance increases as η_3 increases for both (P1, C1) and (P2, C1). Also, through simulation we notice that as η_3 increases to 0.1 the AUVs cannot move towards their destinations within the given time. They have to stay away from each other due to the large η_3 while maintaining network integrity which is hard to achieve. As a result, they just move around to find optimal locations. Moreover, by using (30) we can ensure that collisions (two AUVs have the same location) can be avoided and the minimum distance is always larger than 0. The minimum distance does not increase as η_3 increases. This is due to the wireless energy transfer, which drives AUVs and the mobile charger close.

In Fig. 12 we show the received energy associated with the simulation in Fig. 11. As we can see, the received energy is affected by the minimum distance in Fig. 11. For (P1, C1), the minimum distance is almost a constant and the associated received energy is also stable. For (P2, C1), when $\eta_3 = 0.0006$ the minimum distance is the largest, and the received energy is the smallest. Note that, the minimum distance and the received energy depend on the motion policy, the initial locations, and destinations.

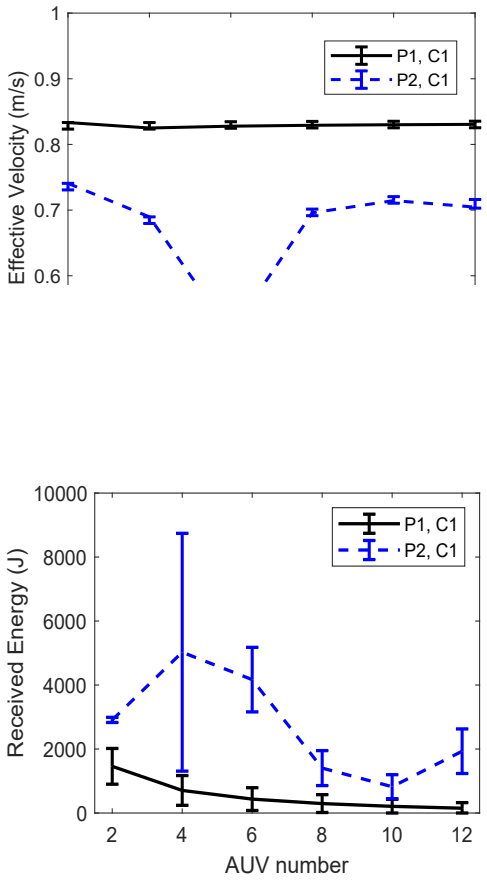

Fig. 14. Received energy for AUV swarms with 2 to 12 AUVs using Policy 1 in Case 1 (P1, C1) and Policy 2 in Case 1 (P2, C1).

destinations are set following the same approach as that when the number is 4. The effective velocity in Fig. 13 indicates that using (P1, C1) the velocity is not affected by AUV number since they do not cooperate with the mobile charger while using (P2, C1) the velocity is affected by the AUV number. The swarm moves fast when the AUV number is extremely large or small. When the number is small, all AUVs are around the mobile charger, it is easy to meet the network constraints, while when the number is large since some of the AUVs are far from the mobile charger, they cannot receive sufficient energy and they move fast towards their destinations which drives the whole swarm forward. When the AUV number is in the middle, i.e., 6 in the figure, AUVs move around the mobile charger to harvest more energy and the effective velocity becomes smaller.

The received energy is shown in Fig. 14. As we can see, for (P1, C1) the received energy monotonically decreases as the number increases, while for (P2, C1) the standard deviation is large which means the fairness is poor. But, generally, the trend is the same, i.e., the more AUVs the smaller received energy.

VI. Conclusion

Swarm AUVs is an important approach to explore and monitor underwater environments. To provide a continuous energy supply, we propose to use mobile chargers to wirelessly recharge AUVs. In this way, AUVs can conduct tasks persistently. In this paper, we first prove that using tri-axis coils we can obtain reliable wireless energy transfer and wireless communication without experiencing orientation losses. We develop optimal transmission and receiving algorithms. Then, we derive a simple underwater magnetic induction channel model by using tri-axis coils. The developed channel model is used to design efficient and distributed motion potential functions, upon which we find the optimal velocity for each AUV. We provide two wireless energy transfer policies and numerically evaluate their performances. Our results show that it is feasible to adopt wireless mobile charging in underwater and the proposed solutions are efficient to maintain wireless network integrity and high wireless energy transfer efficiency while accomplishing AUVs' tasks.

Appendix A
Magnetic Fields in Cartesian Coordinates

The magnetic fields generated by x, y, and z orientated coils in the underwater environment considering water-air interface are expressed in Cylindrical Coordinates, which can be written as $\boldsymbol{H} = [\boldsymbol{h}^x, \boldsymbol{h}^y, \boldsymbol{h}^z]$, where $\boldsymbol{h}^i = [h^i_\rho, h^i_\phi, h^i_z]^T$ for $i = x, y$ and z and their expressions are given in [9] and the appendix

in [1]. The model is derived by considering each transmitting coil has a unit current. Thus, by using $\boldsymbol{H}\boldsymbol{u}_m s_m$, we can obtain the magnetic fields in Cylindrical Coordinates, which are generated by a coil with orientation $\boldsymbol{u}_m$ and excitation current s_m. To transform the fields to Cartesian Coordinates, we only need a transform matrix $\boldsymbol{L}$ which is given in [9]. Thus, we have $\boldsymbol{D} = \boldsymbol{L}\boldsymbol{H}$.

APPENDIX B
SIMPLIFICATION OF (21) AND (24)

For the direct path, the magnetic fields generated by a magnetic dipole are given in [48, chap. 5]: $h_r = \frac{jk_2a^2N_cs\cos\theta}{2r^2}[1+\frac{1}{jk_2r}]e^{jk_2r}$, $h_\theta = \frac{-k_2^2a^2N_cs\sin\theta}{4r}[1+\frac{1}{jk_2r}-\frac{1}{(k_2r)^2}]e^{jk_2r}$, and $h_\phi = 0$. We consider the dominant terms when $k_2r \ll 1$ and $k_2r \gg 1$, which are $h_r = \frac{a^2N_cs}{2r^3}e^{jk_2r}$ and $h_\theta = \frac{-k_2^2a^2N_cs}{4r}e^{jk_2r}$, respectively. Note that, the angle is neglected since by using tri-axis coils, we can compensate the orientation loss. Then, by using the two dominant terms, we can obtain (21). For the lateral wave, a simplified model is given in [1] and the assumption is that the distance between a transmitter and a receiver is much larger than their depth. Similarly, we can neglect angles by using tri-axis coils. Also, since the absolute value of the propagation constant of water k_2 is much larger than that of air k_1 due to the high permittivity and conductivity of water, $|k_2/k_1| \gg 1$. By using this property, we can find the dominant terms in ρ, ϕ, and z direction, which are given in (24).

REFERENCES

[1] H. Guo, Z. Sun, and P. Wang, "On reliability of underwater magnetic induction communications with tri-axis coils," in *IEEE International Conference on Communications (ICC)*, May 2019, pp. 1–6.

[2] N. Saeed, A. Celik, T. Al-Naffouri, and M.-S. Alouini, "Energy harvesting hybrid acoustic-optical underwater wireless sensor networks localization," *Sensors*, vol. 18, no. 1, p. 51, 2018.

[3] J. Liu, Z. Wang, Z. Peng, J.-H. Cui, and L. Fiondella, "Suave: Swarm underwater autonomous vehicle localization," in *IEEE INFOCOM IEEE Conference on Computer Communications*. IEEE, 2014, pp. 64–72.

[4] A. Alvarez, A. Caffaz, A. Caiti, G. Casalino, L. Gualdesi, A. Turetta, and R. Viviani, "Folaga: A low-cost autonomous underwater vehicle combining glider and AUV capabilities," *Ocean Engineering*, vol. 36, no. 1, pp. 24–38, 2009.

[5] I. F. Akyildiz, P. Wang, and Z. Sun, "Realizing underwater communication through magnetic induction," *IEEE Communications Magazine*, vol. 53, no. 11, pp. 42–48, 2015.

[6] S. Soylu, B. J. Buckham, and R. P. Podhorodeski, "Dynamics and control of tethered underwater-manipulator systems," in *OCEANS 2010 MTS/IEEE SEATTLE*. IEEE, 2010, pp. 1–8.

[7] N. Saeed, A. Celik, T. Y. Al-Naffouri, and M.-S. Alouini, "Underwater optical wireless communications, networking, and localization: A survey," *Ad Hoc Networks*, p. 101935, 2019.

[8] B. Gulbahar and O. B. Akan, "A communication theoretical modeling and analysis of underwater magneto-inductive wireless channels," *IEEE Transactions on Wireless Communications*, vol. 11, no. 9, pp. 3326–3334, 2012.

[9] H. Guo, Z. Sun, and P. Wang, "Multiple frequency band channel modeling and analysis for magnetic induction communication in practical underwater environments," *IEEE Transactions on Vehicular Technology*, vol. 66, no. 8, pp. 6619–6632, 2017.

[10] M. C. Domingo, "Magnetic induction for underwater wireless communication networks," *IEEE Transactions on Antennas and Propagation*, vol. 60, no. 6, pp. 2929–2939, 2012.

[11] Y. Li, S. Wang, C. Jin, Y. Zhang, and T. Jiang, "A survey of underwater magnetic induction communications: Fundamental issues, recent advances, and challenges," *IEEE Communications Surveys Tutorials*, vol. 21, no. 3, pp. 2466–2487, thirdquarter 2019.

[12] A. LiVecchi, A. Copping, D. Jenne, A. Gorton, A. Preus, G. Gill, R. Robichaud, R. Green, S. Geerlofs, S. Gore *et al.*, "Powering the blue economy; exploring opportunities for marine renewable energy in maritime markets," *US Department of Energy, Office of Energy Efficiency and Renewable Energy. Washington, DC*, 2019.

[13] J. Garnica, R. A. Chinga, and J. Lin, "Wireless power transmission: From far field to near field," *Proceedings of the IEEE*, vol. 101, no. 6, pp. 1321–1331, 2013.

[14] A. Karalis, J. D. Joannopoulos, and M. Soljačić, "Efficient wireless non-radiative mid-range energy transfer," *Annals of physics*, vol. 323, no. 1, pp. 34–48, 2008.

[15] B. L. Cannon, J. F. Hoburg, D. D. Stancil, and S. C. Goldstein, "Magnetic resonant coupling as a potential means for wireless power transfer to multiple small receivers," *IEEE transactions on power electronics*, vol. 24, no. 7, pp. 1819–1825, 2009.

[16] A. Shaw, A. Al-Shamma'a, S. Wylie, and D. Toal, "Experimental investigations of electromagnetic wave propagation in seawater," in *2006 European Microwave Conference*. IEEE, 2006, pp. 572–575.

[17] K. Fotopoulou and B. W. Flynn, "Wireless power transfer in loosely coupled links: Coil misalignment model," *IEEE Transactions on Magnetics*, vol. 47, no. 2, pp. 416–430, 2010.

[18] A. Markham and N. Trigoni, "Magneto-inductive networked rescue system (miners): taking sensor networks underground," in *Proceedings of the 11th international conference on Information Processing in Sensor Networks*. ACM, 2012, pp. 317–328.

[19] H. Guo, Z. Sun, and P. Wang, "Channel modeling of mi underwater communication using tri-directional coil antenna," in *Global Communications Conference (GLOBECOM), 2015 IEEE*. IEEE, 2015, pp. 1–6.

[20] S. Kisseleff, I. F. Akyildiz, and W. Gerstacker, "Beamforming for magnetic induction based wireless power transfer systems with multiple receivers," in *2015 IEEE Global Communications Conference (GLOBECOM)*. IEEE, 2015, pp. 1–7.

[21] L. Pessoa, M. Pereira, H. Santos, and H. Salgado, "Simulation and experimental evaluation of a resonant magnetic wireless power transfer system for seawater operation," in *OCEANS 2016-Shanghai*. IEEE, 2016, pp. 1–5.

[22] V. Bana, M. Kerber, G. Anderson, J. D. Rockway, and A. Phipps, "Underwater wireless power transfer for maritime applications," in *2015 IEEE Wireless Power Transfer Conference*. IEEE, 2015, pp. 1–4.

[23] J. B. Joslin, E. D. Cotter, P. G. Murphy, P. J. Gibbs, R. J. Cavagnaro, C. R. Crisp, A. R. Stewart, B. Polagye, P. S. Cross, and E. Hjetland, "The wave-powered adaptable monitoring package: hardware design, installation, and deployment," in *12th European Wave and Tidal Energy Conference*, 2019.

[24] X. Shi, H. Lee, V. Jain, and J. R. Smith, "Coil geometry optimization for wireless power delivery to moving receivers," in *2018 IEEE Wireless Power Transfer Conference (WPTC)*. IEEE, 2018, pp. 1–4.

[25] M. M. Zavlanos, A. Ribeiro, and G. J. Pappas, "Network integrity in mobile robotic networks," *IEEE Transactions on Automatic Control*, vol. 58, no. 1, pp. 3–18, 2012.

[26] J. Fink, A. Ribeiro, and V. Kumar, "Robust control for mobility and wireless communication in cyber–physical systems with application to robot teams," *Proceedings of the IEEE*, vol. 100, no. 1, pp. 164–178, 2011.

[27] Y. Yan and Y. Mostofi, "Co-optimization of communication and motion planning of a robotic operation under resource constraints and in fading environments," *IEEE Transactions on Wireless Communications*, vol. 12, no. 4, pp. 1562–1572, 2013.

[28] Y. Kantaros and M. M. Zavlanos, "Global planning for multi-robot communication networks in complex environments," *IEEE Transactions on Robotics*, vol. 32, no. 5, pp. 1045–1061, 2016.

[29] R. Zhang and C. K. Ho, "Mimo broadcasting for simultaneous wireless information and power transfer," *IEEE Transactions on Wireless Communications*, vol. 12, no. 5, pp. 1989–2001, 2013.

[30] B. Arbanas, T. Petrovic, and S. Bogdan, "Consensus protocol for underwater multi-robot system using scheduled acoustic communication," in *2018 OCEANS-MTS/IEEE Kobe Techno-Oceans (OTO)*. IEEE, 2018, pp. 1–5.

[31] J. Yu, C. Wang, and G. Xie, "Coordination of multiple robotic fish with applications to underwater robot competition," *IEEE Transactions on Industrial Electronics*, vol. 63, no. 2, pp. 1280–1288, 2015.

[32] A. C. Kapoutsis, S. A. Chatzichristofis, L. Doitsidis, J. B. de Sousa, J. Pinto, J. Braga, and E. B. Kosmatopoulos, "Real-time adaptive multi-robot exploration with application to underwater map construction," *Autonomous robots*, vol. 40, no. 6, pp. 987–1015, 2016.

[33] Q. Yang and S.-J. Yoo, "Optimal UAV path planning: Sensing data acquisition over IoT sensor networks using multi-objective bio-inspired algorithms," *IEEE Access*, vol. 6, pp. 13 671–13 684, 2018.

[34] T. Zeng, M. Mozaffari, O. Semiari, W. Saad, M. Bennis, and M. Debbah, "Wireless communications and control for swarms of cellular-connected UAVs," in *2018 52nd Asilomar Conference on Signals, Systems, and Computers*. IEEE, 2018, pp. 719–723.

[35] Y. Zeng and R. Zhang, "Energy-efficient UAV communication with trajectory optimization," *IEEE Transactions on Wireless Communications*, vol. 16, no. 6, pp. 3747–3760, 2017.

[36] S. Suman, S. Kumar, and S. De, "UAV-assisted RFET: A novel framework for sustainable WSN," *IEEE Transactions on Green Communications and Networking*, vol. 3, no. 4, pp. 1117–1131, 2019.

[37] ——, "UAV-assisted RF energy transfer," in *2018 IEEE International Conference on Communications (ICC)*. IEEE, 2018, pp. 1–6.

[38] J. Xu, Y. Zeng, and R. Zhang, "UAV-enabled wireless power transfer: Trajectory design and energy optimization," *IEEE Transactions on Wireless Communications*, vol. 17, no. 8, pp. 5092–5106, 2018.

[39] B. Griffin and C. Detweiler, "Resonant wireless power transfer to ground sensors from a UAV," in *2012 IEEE international conference on robotics and automation*. IEEE, 2012, pp. 2660–2665.

[40] M. T. Dabiri, H. Safi, S. Parsaeefard, and W. Saad, "Analytical channel models for millimeter wave UAV networks under hovering fluctuations," *IEEE Transactions on Wireless Communications*, vol. 19, no. 4, pp. 2868–2883, 2020.

[41] S. Suman, S. Kumar, and S. De, "Impact of hovering inaccuracy on UAV-aided RFET," *IEEE Communications Letters*, vol. 23, no. 12, pp. 2362–2366, 2019.

[42] J. Stephan, J. Fink, V. Kumar, and A. Ribeiro, "Concurrent control of mobility and communication in multirobot systems," *IEEE Transactions on Robotics*, vol. 33, no. 5, pp. 1248–1254, 2017.

[43] E. Kelasidi, K. Y. Pettersen, and J. T. Gravdahl, "Energy efficiency of underwater robots," *IFAC-PapersOnLine*, vol. 48, no. 16, pp. 152–159, 2015.

[44] ——, "Energy efficiency of underwater snake robot locomotion," in *2015 23rd Mediterranean Conference on Control and Automation (MED)*. IEEE, 2015, pp. 1124–1131.

[45] T. T. J. Prestero, "Verification of a six-degree of freedom simulation model for the remus autonomous underwater vehicle," Ph.D. dissertation, Massachusetts institute of technology, 2001.

[46] N. Yang, D. Chang, M. R. Amini, M. Johnson-Robersor, and J. Sun, "Energy management for autonomous underwater vehicles using economic model predictive control," in *2019 American Control Conference (ACC)*, July 2019, pp. 2639–2644.

[47] R. King, "Electromagnetic surface waves: New formulas and applications," *IEEE transactions on antennas and propagation*, vol. 33, no. 11, pp. 1204–1212, 1985.

[48] C. A. Balanis, *Antenna theory: analysis and design*. John wiley & sons, 2016.

[49] J. Jadidian and D. Katabi, "Magnetic MIMO: How to charge your phone in your pocket," in *Proceedings of the 20th annual international conference on Mobile computing and networking*, 2014, pp. 495–506.

[50] G. Yang, M. R. V. Moghadam, and R. Zhang, "Magnetic mimo signal processing and optimization for wireless power transfer," *IEEE Transactions on Signal Processing*, vol. 65, no. 11, pp. 2860–2874, 2017.

[51] H.-D. Lang, A. Ludwig, and C. D. Sarris, "Convex optimization of wireless power transfer systems with multiple transmitters," *IEEE Transactions on Antennas and Propagation*, vol. 62, no. 9, pp. 4623–4636, 2014.

[52] T. M. Cover and J. A. Thomas, *Elements of information theory*. John Wiley & Sons, 2012.

[53] P. Grover and A. Sahai, "Shannon meets tesla: Wireless information and power transfer," in *2010 IEEE international symposium on information theory*. IEEE, 2010, pp. 2363–2367.

[54] A. Goldsmith, *Wireless communications*. Cambridge university press, 2005.

[55] M. Grant and S. Boyd, "CVX: Matlab software for disciplined convex programming, version 2.1," http://cvxr.com/cvx, Mar. 2014.

[56] E. Rimon and D. E. Koditschek, "Exact robot navigation using artificial potential functions," *IEEE Transactions on Robotics and Automation*, vol. 8, no. 5, pp. 501–518, Oct 1992.

[57] X. Tan, Z. Sun, and I. F. Akyildiz, "Wireless Underground Sensor Networks: MI-based communication systems for underground applications." *IEEE Antennas and Propagation Magazine*, vol. 57, no. 4, pp. 74–87, 2015.

[58] J. J. Kuffner and S. M. LaValle, "RRT-connect: An efficient approach to single-query path planning," in *Proceedings 2000 ICRA. Millennium Conference. IEEE International Conference on Robotics and Automation. Symposia Proceedings (Cat. No. 00CH37065)*, vol. 2. IEEE, 2000, pp. 995–1001.

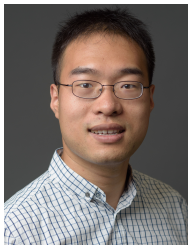

Hongzhi Guo (S'12-M'17) received his Ph.D. degree from University at Buffalo, the State University of New York in 2017, and his M.S. degree from Columbia University in 2013, both in Electrical Engineering. Currently, he is an Assistant Professor of Electrical Engineering at Norfolk State University. His broad research agenda is to develop the foundations for wireless sensor networks and networked robotics to automate dangerous, dirty, dull tasks in extreme environments, such as underground and underwater. He received the NSF CRII award in 2020, the Jeffress Trust Awards Program in Interdisciplinary Research in 2020, the Best Demo Award from IEEE INFOCOM in 2017, and the Exemplary Reviewer from IEEE Transactions on Wireless Communications in 2017.

Zhi Sun (S'06-M'11-SM'19) received the B.S. degree in telecommunication engineering from Beijing University of Posts and Telecommunications (BUPT), Beijing, China, in 2004, the M.S. degree in electronic engineering from Tsinghua University, Beijing, in 2007, and the Ph.D. degree in electrical and computer engineering from the Georgia Institute of Technology, Atlanta, GA, USA, in 2011. He was a Postdoctoral Fellow with Georgia Institute of Technology from 2011 to 2012. In 2012, he joined the Department of Electrical Engineering, University at Buffalo, The State University of New York, Buffalo, NY, USA, as an Assistant Professor. He is currently an Associate Professor with University at Buffalo. His research interests include wireless communication and networking in extreme environments, physical-layer security, metamaterial enhanced communication and security, wireless intrabody networks, wireless underground networks, wireless underwater networks, and cyber-physical systems. He was a recipient of the NSF CAREER Award in 2017, the UB Exceptional Scholar—Young Investigator Award in 2017, the Best Demo Award at IEEE Infocom 2017, the Best Paper Award at IEEE Globecom in 2010, the BWN Researcher of the Year Award at the Georgia Institute of Technology in 2009, and the Outstanding Graduate Award at Tsinghua University in 2007. He serves as an Editor for the IEEE TRANSACTIONS ON WIRELESS COMMUNICATIONS and Computer Networks (Elsevier). He is a senior member of IEEE.

Pu Wang received the B.Eng. degree in electrical engineering from the Beijing Institute of Technology, China, in 2003, the M.Eng. degree in electrical and computer engineering from the Memorial University of Newfoundland, Canada, in 2008, and the Ph.D. degree in electrical and computer engineering from the Georgia Institute of Technology, Atlanta, GA, USA, in August 2013, under the guidance of Prof. I. F. Akyildiz. He was an Assistant Professor with the Department of Electrical Engineering and Computer Science, Wichita State University, from 2013 to 2017. He is currently an Assistant Professor with the Department of Computer Science, the University of North Carolina at Charlotte. His current research interests include machine learning, and stochastic optimization of networked systems, with applications in software-defined networking, cyber-physical systems, the Internet of Things, wireless sensor networks, cognitive radio networks, and electromagnetic nanonetworks.